UNCLASSIFIED

SECURITY CLASSIFICATION OF THIS PAGE

REPORT DOCUMENTATION PAGE	Form Approved OMB No. 0704-0188

1a. REPORT SECURITY CLASSIFICATION Unclassified	1b. RESTRICTIVE MARKINGS

2a. SECURITY CLASSIFICATION AUTHORITY	3. DISTRIBUTION/AVAILABILITY OF REPORT
2b. DECLASSIFICATION/DOWNGRADING SCHEDULE	Approved for public release; distribution unlimited.

4. PERFORMING ORGANIZATION REPORT NUMBER(S) HDL-TR-2184	5. MONITORING ORGANIZATION REPORT NUMBER(S)

6a. NAME OF PERFORMING ORGANIZATION Harry Diamond Laboratories	6b. OFFICE SYMBOL (If applicable) SLCHD-NW-EP	7a. NAME OF MONITORING ORGANIZATION

6c. ADDRESS (City, State, and ZIP Code) 2800 Powder Mill Road Adelphi, MD 20783-1197	7b. ADDRESS (City, State, and ZIP Code)

8a. NAME OF FUNDING/SPONSORING ORGANIZATION U.S. Army Laboratory Command	7b. OFFICE SYMBOL (If applicable) AMSLC	9. PROCUREMENT INSTRUMENT IDENTIFICATION NUMBER

8c. ADDRESS (City, State, and ZIP Code) 2800 Powder Mill Road Adelphi, MD 20783-1145	10. SOURCE OF FUNDING NUMBERS			
	PROGRAM ELEMENT NO. 6.11.02	PROJECT NO.	TASK NO.	WORK UNIT ACCESSION NO.

11. TITLE (Include Security Classification)

Mobility of Nonequilibrium Conduction Electrons in Air

12. PERSONAL AUTHOR(S)
William T. Wyatt, Jr., and Christopher S. Kenyon

13a. TYPE OF REPORT Final	13b. TIME COVERED FROM Oct 88 TO Sept 89	14. DATE OF REPORT (Year, Month, Day) June 1990	15. PAGE COUNT 46

16. SUPPLEMENTARY NOTATION
AMS code: 611102.H440011
HDL project: AE17E3

17. COSATI CODES			18. SUBJECT TERMS (Continue on reverse if necessary and identify by block number)
FIELD	GROUP	SUB-GROUP	Plasma, conductivity, transients, variational principle, electron
20	9		

19. ABSTRACT (Continue on reverse if necessary and identify by block number)

An integro-differential equation is derived describing the time evolution of the electron energy distribution function in a gas in a transient electric field. A finite-difference approximation and a time-stepping algorithm using matrix-vector techniques are devised to solve the integro-differential equation. An extensive published cross section set is added to the time-stepping algorithm, enabling one to calculate realistic energy distribution functions in air. Also described is a projection method that allows computation of electron swarm properties such as "collision volume" (inversely related to mobility) using measured data for equilibrium distributions. This projection method is shown to have desirable variational properties in calculating the swarm properties. We compare orthogonal and nonnegative projection methods with conventional techniques for their ability to reduce error in estimates of collision volume arising from cross-section-induced error in the energy distribution function. We found that a single-vector projection with "cleanup" of approximation error performs best, leading to significant reduction of collision volume error when the distribution function maximum occurs

20. DISTRIBUTION/AVAILABILITY OF ABSTRACT ☒ UNCLASSIFIED/UNLIMITED ☐ SAME AS RPT. ☐ DTIC USERS	21. ABSTRACT SECURITY CLASSIFICATION Unclassified	
22a. NAME OF RESPONSIBLE INDIVIDUAL William T. Wyatt, Jr.	22b. TELEPHONE (Include Area Code) (703) 490-2303	22c. OFFICE SYMBOL SLCHD-NW-EP

DD Form 1473, JUN 86   Previous editions are obsolete.

SECURITY CLASSIFICATION OF THIS PAGE
UNCLASSIFIED

i

19. Abstract cont'd

at not more than about 0.1 eV. Other projections perform poorly compared to conventional methods of calculating swarm collision volume, because of inherent dependence of the projection basis of equilibrium distributions and resulting ill-conditioning of the projection matrix.

Accesion For	
NTIS CRA&I	☑
DTIC TAB	☐
Unannounced	☐
Justification	
By	
Distribution /	
Availability Codes	
Dist	Avail and / or Special
A-1	

Table of Contents

List of Illustrations

List of Tables

1 Introduction and Motivation

1.1 Nonequilibrium Mobility by Projection onto an Equilibrium Basis

The mobility of conduction electrons in air subjected to an electric field changing rapidly in a nanosecond or less is difficult to measure or calculate. The conduction electrons do not attain an equilibrium state in such a short time. Steady-state "swarm" measurements are readily available, but only approximate nonequilibrium values. Approaches using energy-dependent momentum exchange cross-section data with a conduction electron velocity distribution function are hampered by incomplete cross-section data. In this work, we project the time-dependent energy distribution function onto a basis composed of equilibrium energy distribution functions and use equilibrium mobilities to construct a nonequilibrium mobility. The method is evaluated as a possible means of avoiding error in the energy distribution function arising from incomplete or erroneous cross-section data.

Conduction electron mobility can be expressed in terms of an effective momentum exchange cross-section as[1] [pp 72, 115, 206, 527]

$$\mu = \frac{qW\,10^{-3}}{mu A_n \rho Q_m}, \tag{1a}$$

or

$$\mu = \frac{q}{mu N Q_m}, \tag{1b}$$

where

μ = electron mobility (in $m^2/V\ s$),

Q_m = effective momentum exchange cross-section (in $m^2/molecule$),

q = magnitude of the electron charge (1.60×10^{-19} C),

W = gas molecular weight (28.8 kg/Mole, 1 Mole = 1000 mole),

m = electron mass (9.11×10^{-31} kg),

u = electron speed (m/s) for electron kinetic energy E (in J),

A_n = Avogadro's number ($6.03 \times 10^{23}/mole$),

ρ = gas density (in kg/m^3), and

N = gas molecular density (in $molecules/m^3$).

The macroscopic conduction electron mobility, averaged over the ensemble electron energies (which we denote by a caret), is written as

$$\hat{\mu} = \frac{q}{mN \int u(E) Q_m(E) f(E)\, dE} \tag{2}$$

---

[1] Huxley, L. G. H., and R. W. Crompton, *The Diffusion and Drift of Electrons in Gases*, John Wiley and Sons, New York (1974).

I

where $f(E)$ is the time-independent (equilibrium) energy distribution of electron kinetic energies. We may, for convenience, parameterize $\hat{\mu}$ as a function of the ensemble average electron energy $\hat{E}$, which is a monotonic function of the ambient (time-independent) electric field strength. Let us define

$$K(E) = u(E)Q_m(E) \tag{3}$$

and the ensemble average $\hat{K}(\hat{E})$ as

$$\hat{K}(\hat{E}) = \int u(E)Q_m(E)f(E)\,dE. \tag{4}$$

The variables K and $\hat{K}$, which we shall call "collision volume," are in units of volume per unit time and, when multiplied by the density of target molecules, yield the momentum exchange collision frequency v_m.

The ensemble average collision volume $\hat{K}$ can be written as a function of time

$$\hat{K}(t) = \int K(E)f(E,t)\,dE \tag{5}$$

where the integral is carried over all electron energies, and $f(E,t)$ is the time-dependent energy distribution function (in electrons per unit energy). We assert without proof that an infinite basis exists complete for any $f(E,t)$, consisting of the family of equilibrium energy distribution functions $\phi(E, \Lambda)$ for all nonnegative values of the parameter Λ. The parameter Λ may be chosen to be some monotonic characteristic of the distribution, such as magnitude of the electric field strength or average energy. We discretize the basis for parameter values $\Lambda = \Lambda_i$ and approximate $f(E,t)$ by

$$f(E,t) = \sum_i a_i(t)\,\phi(E, \Lambda_i), \tag{6}$$

which defines time-dependent coefficients $a_i(t)$. (This definition does not uniquely define the $a_i(t)$, however, because the basis is not orthogonal. Orthogonality will be considered in section 3.1.) Substituting this basis into equation (5) we obtain

$$\begin{aligned}
\hat{K}(t) &= \int \sum_i K(E)a_i(t)\phi(E, \Lambda_i)\,dE, \\
&= \sum_i a_i(t) \int K(E)\phi(E, \Lambda_i)\,dE.
\end{aligned} \tag{7}$$

The ensemble average collision volume for any equilibrium distribution having parameter value Λ_i is

$$\hat{K}(\Lambda_i) = \int K(E)\phi(E, \Lambda_i)\,dE. \tag{8}$$

The ensemble average collision volume $\hat{K}$ can be easily obtained from "swarm" measurements of electron mobility, which are aimed at taking data for equilibrium energy distributions. By substitution of equation (8) into equation (7) we obtain

2

$$\hat{K}(t) = \sum_i a_i(t) \hat{K}(\Lambda_i). \tag{9}$$

Thus the time-dependent ensemble average collision volume can be obtained from equilibrium ensemble average collision volumes and a knowledge of the $a_i(t)$ describing the time-dependent energy distribution. Alternatively, the same data can be derived from the (energy-dependent) momentum exchange collision cross-section and the time-dependent energy distribution itself. Unfortunately these quantities are not known accurately for all energies.

The motivation for the current work is the possibility that the coefficients $a_i(t)$ can be determined more accurately than either $f(E,t)$ or $\phi(E, \Lambda_i)$, and also more accurately than the collision volume data $K(E)$ upon which they are based. Under certain conditions, the coefficients $a_i(t)$ are stationary with respect to variation of $K(E)$ (due to a variational principle). For example, this occurs when the time-dependent electron energy distribution function is close to an equilibrium energy distribution function. More generally, stationary behavior can be expected when the time-dependent function can be approximated by a set of linearly independent equilibrium functions. If indeed the $a_i(t)$ can be determined more accurately, then the ensemble average collision volume $\hat{K}(\Lambda_i)$ and the ensemble average mobility $\hat{\mu}$ can also be determined more accurately than by direct integration of equation (5).

1.2 Relationship to a Variational Principle

Define a linear operator **L** that advances the energy distribution function $f(E,t)$ one time-step:

$$\mathbf{L}f(E,t) = f(E,t + \Delta t). \tag{10}$$

The equilibrium energy distribution function is defined by

$$\mathbf{L}g(E) = g(E) \tag{11}$$

for a fixed electric field strength. Clearly $g(E)$ is an eigenvector of **L** associated with the eigenvalue unity. A well-known result[2] shows that eigenvalues may be derived from a variational principle as

$$\lambda = \frac{\displaystyle\int [\mathbf{L}f(x)]f(x)\,dx}{\displaystyle\int f^2(x)\,dx} \tag{12}$$

and that this expression for λ is stationary (second-order accuracy) with respect to variations in $f(x)$.

Identify the $g(E)$ that has the largest projection onto $f(E,t)$, i. e., with the largest $\alpha(t)$ defined by

$$\alpha(t) = \frac{\displaystyle\int f(E,t)g(E)\,dE}{\displaystyle\int g^2(E)\,dE}. \tag{13}$$

---

[2] Morse, P. M., and H. Feshbach, *Methods of Theoretical Physics*, McGraw-Hill Book Company, Inc., New York (1953), Volume 2, pp 1108f.

Repeated applications of L to $f(E,t)$ produce new $f(E,t + \Delta t)$ that grow closer to the equilibrium solution $g(E)$

$$L^n f(E,t) = g(E) + \delta g(E,t), \tag{14}$$

where $\delta g(E,t)$ is a differential variation of function g, such that

$$\lim_{n \to \infty} \delta g(E,t) = 0. \tag{15}$$

Now define an operator L^{-1} that is the inverse of L. We observe that repeated applications of L^{-1} to $g(E) + \delta g(E,t)$ produce

$$\left(L^{-1}\right)^n [g(E) + \delta g(E,t)] = f(E,t). \tag{16}$$

If we now define operator M for some large n,

$$M = \left(L^{-1}\right)^n, \tag{17}$$

we see that

$$\lambda_n \simeq \frac{\int \{M[g(E) + \delta g(E,t)]\} \, [g(E) + \delta g(E,t)] \, dE}{\int [g(E) + \delta g(E,t)]^2 \, dE} \tag{18}$$

is in the form of equation (12) for operator M and its approximate eigenvector $g(E) + \delta g(E,t)$. The approximate eigenvalue λ_n is accurate to second order by the variational principle cited. However we can make $\delta g(E,t)$ arbitrarily small by increasing n. Using

$$M[g(E) + \delta g(E,t)] = f(E,t) \tag{19}$$

and allowing $n \to \infty$ so that $\delta g(E,t) \to 0$, we rewrite equation (18) as

$$\lambda_\infty = \frac{\int f(E,t)g(E)dE}{\int g^2(E) \, dE}. \tag{20}$$

Comparing this with equation (13) we see that

$$\alpha(t) = \lambda_\infty \tag{21}$$

and that equation (13) is variational also.

The remainder

$$r(E,t) = f(E,t) - \alpha(t)g(E) \tag{22}$$

is orthogonal to $\alpha(t)g(E)$, as can be shown by multiplying equation (22) by $g(E)$ and integrating over energy. If $r(E,t)$ is small compared to $f(E,t)$ (that is, if $g(E)$ is "close" to $f(E,t)$) then we expect that equation (9) will provide better estimates of $\hat{K}(t)$ than equation (5), given some uncertainty in the calculation of $f(E,t)$ due to error in electron collision cross-section data. This expectation is based on the variational property of equation (13). Even if $r(E,t)$ is not small, it may be "close" to another equilibrium energy distribution function $g'(E)$ that is nearly orthonormal to $g(E)$:

$$\int g^2(E) \, dE \gg \int g(E)g'(E) \, dE. \tag{23}$$

4

For instance, if $g(E)$ is concentrated at low energy and $g'(E)$ is concentrated at high energy, then they will be nearly orthonormal. If equation (23) holds, the process may be repeated to obtain

$$\alpha'(t) = \frac{\displaystyle\int r(E,t)g'(E)\,dE}{\displaystyle\int [g'(E)]^2\,dE} \qquad (24)$$

which has similar, though possibly weaker, variational properties. Clearly the process may be continued in a manner similar to a Gram-Schmidt orthogonalization procedure. The successive projection coefficients will possess (nearly) variational properties so long as the successive $g, g', \ldots$ are (nearly) orthonormal.

2 Solution Method for Energy Distribution Function

2.1 Energy Diffusion Equation

To demonstrate the projection technique described, we need a method of calculating equilibrium and time-dependent energy distribution spectra for free electrons in air. Historically most transport models of free electrons in air have been based on a distribution function which describes electron number density in phase space, that is, as a function of time, position, and velocity (or momentum) in three dimensions. Usually the Maxwell-Boltzmann equation or some variant is used to define that distribution function[1] [chapter 2]. For the present effort we choose a simpler formulation based on a distribution function which depends only on time and electron energy. Derived from the integro-differential form of the Boltzmann transport equation, this formulation will be adequate to develop a time-dependent nonequilibrium energy distribution of electron number density and to demonstrate the projection of the time-dependent distribution onto a (more or less) complete set of equilibrium distributions. The projection will permit the calculation of the nonequilibrium mobility from the equilibrium basis.

Because the position and direction of any free electron in a uniform gas are randomized (except for drift) after a few collisions, electron energy remains the principal feature of an electron swarm (together with density, which we assume is constant). Certain macroscopic parameters (mobility, diffusion coefficient, etc.) can be calculated from the electron energy distribution function. When the energy distribution function equilibrates or arrives at a steady state, the equilibrium energy distribution can be used to calculate equilibrium macroscopic parameters.[3,4]

We will develop an equation for the electron energy distribution function, the "energy diffusion equation," with time and electron energy as independent parameters. Its terms are obtained by balancing energy gains and losses

---

[3] Frost, L. S., and A. V. Phelps, Rotational excitation and momentum transfer cross-sections for electrons in H_2 and N_2 from transport coefficients, Phys. Rev. 127 (1962), 1621.

[4] Phelps, L. V., and L. C. Pitchford, Anisotropic scattering of electrons by N_2 and its effect on electron transport, Phys. Rev. A 31 (1985), 2932.

through various collisions and through interaction with the electric field (zero magnetic field is assumed). Spatial uniformity is assumed, so spatial derivatives are omitted. For ambient electric fields varying, say, on a scale of a tenth of a nanosecond, spatial derivatives can be neglected if electron mean free paths are much less than a few centimeters. In fact the mean free paths are of the order of microns for sea-level air. The integro-differential form of the Boltzmann transport equation is the starting point in the derivation. Electron ballistic equations in the electric field are derived and incorporated into the transport equation. Reduction of the transport integrals to first- and second-order differential forms will be shown for the case of "scattering" by the electric field. Finally integral terms will be added for scattering by collision with molecules. Carron[5] [p 9] has exhibited the energy diffusion equation as obtained from the equation for the lowest harmonic of the electron velocity distribution function. Our derivation is based on a Taylor series expansion of the collision integral and suggests how higher order effects might be estimated. However, our emphasis here is on the projection method rather than on the energy diffusion equation itself.

In the derivation it will be assumed that scattering is isotropic, and therefore that the direction cosine of the emergent electron with respect to the ambient electric field is uniformly distributed on the interval $(-1, +1)$. This is a very good approximation for elastic scattering[4] but less accurate for inelastic scatters. Should it be necessary, the probability distribution function for angular distribution can easily be expanded to include an additional Legendre polynomial (or more), becoming $1 + b_1 x + \cdots$, if sufficient data for the b_i are available. Obtaining the electron drift velocity from the electron density function in phase space depends critically upon using a two-term (or more) harmonic expansion of the angular distribution of the electron velocity (because drift velocity is closely allied with the second term). But obtaining the number density in time-energy space, as done here, does not depend on the second harmonic term for drift velocity to be exhibited. Both drift and diffusion are present with only one harmonic term, because the harmonic expansion is for the direction of the electron as it emerges from a collision, not for the direction of motion of the electron at any later time.

Consider an electron in air with electric field $\vec{\varepsilon}$. The electron's velocity is $\vec{u}$ and energy $E = \frac{1}{2}mu^2$. Resolve the velocity into a component parallel to $\vec{\varepsilon}$

$$\vec{u}_\| = \tilde{\varepsilon}(\vec{u} \cdot \tilde{\varepsilon})$$

and a component normal to $\vec{\varepsilon}$

$$\vec{u}_\perp = |\vec{u} \times \tilde{\varepsilon}|$$

where $\tilde{\varepsilon}$ is the unit vector parallel to $\vec{\varepsilon}$. We define the direction cosine μ_ε for $\vec{u}$ relative to $\tilde{\varepsilon}$ and obtain

$$u_\| = |\vec{u}_\|| = u\mu_\varepsilon \tag{25a}$$

$$u_\perp = |\vec{u}_\perp| = u\sqrt{1 - \mu_\varepsilon^2}. \tag{25b}$$

The electron will be accelerated in the electric field until it collides with a molecule. Assume that the electric field is essentially constant in the time between collisions. This is certainly true in the equilibrium case in which the

[5] Carron, N. J., On the Calculation of the Electron Energy Spectrum in a Weakly Ionized Gas, Mission Research Corporation Report MRC-R-1055 (30 January 1987).

electric field must be constant for all time. Generally this assumption requires that the electric field change slowly in a collision time (approximately the reciprocal of the momentum exchange collision frequency). After a time t, $u_\perp$ is unchanged and $u_\parallel$ becomes

$$u_\parallel = u\mu_\varepsilon - \frac{q\varepsilon t}{m} \tag{26}$$

if no collision has occurred. If a collision occurs, the electron's direction is effectively randomized, on the assumption of isotropic scattering. The probability of no collision occurring is $e^{-\nu t}$, where ν is the electron collision frequency, which may be a function of energy.

As discussed above, the direction cosine μ_ε is distributed uniformly on the interval $(-1, +1)$. The normalized collision probability (unitless) is

$$dp = \tfrac{1}{2}\nu e^{-\nu t} dt\, d\mu_\varepsilon \tag{27}$$

where the normalization is $\int dp = 1$.

In the usual expression of the transport equation, the differential terms express continuity based on continuous flow processes, with a time derivative plus appropriate divergences of the distribution function. Then all noncontinuous scattering processes are modeled using collision integrals. However, continuous or quasi-continuous processes can also be modeled with integrals instead of divergences, and it is largely a matter of convenience which way to handle a process. In our case, we use integrals to model all scattering processes and derive from the integrals any differential terms we desire, as for scattering by the electric field, for example. Thus the rate of change of the electron energy distribution function $f(E)$ arising from acceleration in the electric field may be written

$$\frac{\partial f(E)}{\partial t} = \int_{E'=0}^{\infty} \nu(E')f(E')\,dp(E', E) - \nu(E)f(E)\int_{E'=0}^{\infty} dp(E, E') \tag{28}$$

where $dp(E', E)$ is the self-adjoint differential probability of an electron accelerating (decelerating) from energy E' to energy E, and *vice versa*. The first integral accounts for electrons arriving at energy E ("in-scatters"), and the second integral accounts for electrons leaving from energy E ("out-scatters"). The self-adjoint property of $dp(E', E)$ does not depend explicitly on the electric field but does require the integral $\int \nu dt$ to be invariant under an exchange of E and E'. A sufficient condition for $\int \nu dt$ to be invariant in this way is for the collision frequency ν to be independent of energy over the range of energy gain or loss experienced by the electron between collisions. However when the electric field is large, the energy gain between collisions can be considerable compared to the initial, unaccelerated electron energy. This may cause significant changes in the collision frequency (or collision cross-section), but does not destroy the invariance of $\int \nu dt$. In the derivation that follows, we will assume that the self-adjoint property applies.

Equation (28) is exact for scattering by the electric field if the integrals are evaluated without approximation. In general this is not possible to do in closed form. One approximation which allows the most general representation of the integrand is to evaluate the integrals by Monte Carlo; this method yields only numerical results and entails statistical error as well, but is widely used. Another approximation which permits analytical representation of results is to expand the integrals as a Taylor series in the energy, a method we will pursue. We want to expand the integrand in a Taylor series

about E, retaining terms only to second order in $E' - E$, which requires that vf be slowly varying compared to dp. However, the energy dependence of v and dp (which also contains v) has not been specified. Assume for the present that v is independent of energy. Then it suffices to expand f only. This causes difficulty when energy-dependent coefficients occur with the final differential forms to be derived, but a way out is offered to overcome the difficulty. Assuming that f varies slowly compared to dp, we thus expand $f(E')$ in a Taylor series about E, retaining terms only to second order:

$$f(E') \simeq f(E) + c_1(E' - E) + c_2(E' - E)^2. \tag{29}$$

Then the in-scatter integral in equation (28) breaks into three terms:

$$\int_{E'=0}^{\infty} f(E')\, dp(E',E) = f(E) \int_{E'=0}^{\infty} dp(E',E)$$
$$+ c_1 \int_{E'=0}^{\infty} (E' - E)\, dp(E',E) + c_2 \int_{E'=0}^{\infty} (E' - E)^2\, dp(E',E). \tag{30}$$

Since $dp(E', E) = dp(E,E')$, the first term cancels the second integral in equation (28), leaving only the second and third terms:

$$\frac{\partial f(E)}{\partial t} = c_1 v \int_{E'=0}^{\infty} (E' - E)\, dp(E', E) + c_2 v \int_{E'=0}^{\infty} (E' - E)^2\, dp(E',E). \tag{31}$$

For brevity define

$$J_n = v \int_{E'=0}^{\infty} (E' - E)^n\, dp(E',E). \tag{32}$$

We now develop a quadrature rule to approximate the right hand side of equation (31) to second order, so that

$$af(E_a) + bf(E_b) + cf(E_c) = c_1 J_1 + c_2 J_2. \tag{33}$$

The coefficient a is a rate coefficient for scattering electrons from energy E_a to energy E_b. The coefficient c is a rate coefficient for scattering electrons from energy E_c to energy E_b. The coefficient b is a rate coefficient for electrons "scattering" from energy E_b to the same energy. Substituting the second-order expansion for $f(E')$ into the latter equation and setting $E_b = E$ yields

$$af(E) + ac_1(E_a - E) + ac_2(E_a - E)^2 + bf(E)$$
$$+ cf(E) + cc_1(E_c - E) + cc_2(E_c - E)^2 = c_1 J_1 + c_2 J_2.$$

Because c_1 and c_2 are arbitrary, this equation requires

$$(a + b + c)f(E) = 0$$
$$c_1[a(E_a - E) + c(E_c - E)] = c_1 J_1$$
$$c_2[a(E_a - E)^2 + c(E_c - E)^2] = c_2 J_2$$

or letting $E_a - E = -\Delta E$ and $E_c - E = \Delta E$ and assuming $f(E) \neq 0$,

$$a = \frac{J_2 - J_1 \Delta E}{2(\Delta E)^2} , \tag{34a}$$

$$b = -\frac{J_2}{(\Delta E)^2} , \tag{34b}$$

$$c = \frac{J_2 + J_1 \Delta E}{2(\Delta E)^2} . \tag{34c}$$

Thus the quadrature form of equation (31),

$$\frac{\partial f(E)}{\partial t} \simeq a f(E - \Delta E) + b f(E) + c f(E + \Delta E), \tag{35}$$

becomes upon substituting equations (34) and rearranging terms,

$$\frac{\partial f(E)}{\partial t} \simeq \frac{J_2}{2(\Delta E)^2} [f(E + \Delta E) - 2f(E) + f(E - \Delta E)]$$
$$+ \frac{J_1}{2\Delta E} [f(E + \Delta E) - f(E - \Delta E)]. \tag{36}$$

Taking the limit as $\Delta E \to 0$ yields the differential equation

$$\frac{\partial f}{\partial t} = \tfrac{1}{2} J_2 \frac{\partial^2 f}{\partial E^2} + J_1 \frac{\partial f}{\partial E} , \tag{37}$$

exhibiting terms for diffusion and heating of the energy distribution function. When solutions are sought through finite-difference methods, equation (36) is sufficient as it stands, although differential equation (37) more succinctly states the physics involved.

If equation (29) is expanded further to higher powers of $E' - E$, then more values of energy will be needed in the quadrature rule expressed by equation (33). This will cause the time derivative of $f(E)$ to be expanded to higher order differences in (36) and higher order derivatives in (37). In fact, by continuing the Taylor series expansion of the "in-scatter" integral it can easily be shown that

$$\frac{\partial f}{\partial t} = \sum_{i=1}^{\infty} \frac{J_i}{i!} \frac{\partial^i f}{\partial E^i} . \tag{38}$$

The importance of such higher order terms depends on their coefficients, which contain J_n. The second-order expansion is central to the diffusion approximation to the transport equation. Carron[5] [p 12] explains on physical grounds why the expansion can reasonably be terminated at second order to obtain the mobility and diffusion coefficient transport parameters.

Evaluation of J_1 and J_2 is tedious and details are not presented here. Using equations (25) and (26) we find that

$$J_1 = \frac{q^2 \varepsilon^2}{3mv} \tag{39}$$

and

$$J_2 = \frac{4q^2 \varepsilon^2 E}{3mv} - \frac{2q^4 \varepsilon^4}{5m^2 v^3} \tag{40}$$

9

where we have made the substitution $E = \frac{1}{2}mu^2$.

If we assume that the collision frequency v equals the momentum exchange collision frequency v_m, which is exactly true for isotropic elastic scattering, we can use the well-known relation

$$\mu = \frac{q}{mv_m} \tag{41}$$

to write

$$J_1 = \frac{1}{3}q\mu\varepsilon^2 \tag{42a}$$

$$J_2 = \frac{4}{3}q\mu\varepsilon^2 E\left[1 - \frac{3}{5}\left(\mu\varepsilon/u\right)^2\right]. \tag{42b}$$

In general, however, the (total) collision frequency is not equal to the momentum exchange collision frequency when (1) elastic scattering is no longer entirely isotropic or (2) inelastic processes occur. Thus, when dealing with higher energies we must be careful in our choice of data for collision frequency. For scattering by the electric field in nitrogen, we have used a combination of elastic momentum exchange data and total (or "effective") momentum exchange data that yields energy distributions in reasonable agreement with published results. For oxygen we simply use total momentum exchange data because of the paucity of separate elastic data. The main issue here is what collision frequency best represents the randomization of the direction of the colliding electron, which is a complicated topic that we shall not discuss in detail.

The quantities J_1 and J_2 turn out to depend on v, which can depend on energy. The derivation requires modification to correctly treat this energy dependence. A close inspection of the integrals shows that the quantity that should be expanded in a Taylor series is f/v instead of f. When f/v is thus expanded, the integrands are valid for energy-dependent v. The effect is to replace each derivative of f with a derivative of f/v. First and second energy derivatives of v appear. Because v varies slowly as a function of E, it is convenient to discard second energy derivatives of v and keep only first energy derivatives of v. This result is used by Carron[5] [p 13]. Thus the heating term becomes

$$\frac{q^2\varepsilon^2}{3m}\ \frac{\partial}{\partial E}\left(\frac{f}{v}\right) \tag{43a}$$

and the diffusion term

$$\frac{2q^2\varepsilon^2}{3m}\left[\frac{\partial}{\partial E}\left(\frac{E}{v}\ \frac{\partial f}{\partial E}\right) - \frac{3q^2\varepsilon^2}{10m}\ \frac{\partial}{\partial E}\left(\frac{1}{v^3}\ \frac{\partial f}{\partial E}\right)\right]. \tag{43b}$$

The heating term describes the convection (through energy space) of electrons from lower to higher energies as they drift through the ambient electric field. Upon examining the diffusion term, we observe that the second term in brackets is smaller than the first term by a factor roughly the square of the electron drift velocity divided by the electron speed. The second term in brackets approximates the influence of terms that are of higher order than the first two terms in the usual Legendre expansion of the velocity distribution function. In derivations of the velocity distribution function, higher order terms than the second are cast away on the assumption that the drift velocity is much smaller than the electron average speed[1] [p 58]. The as-

sumption that in-flight energy changes are much smaller than the initial electron energy, upon which the continuous scattering approximation (eq (37)) is based, is violated when the drift velocity approaches the initial electron speed. This occurs in air at small electron energies because of the small collision cross-section at those energies. For this reason we are forced to omit the second term in brackets when dealing with non-idealized air. Proper inclusion of the second term in brackets would be in the form of an upscatter probability from energy level i to energy level $i+j$ where $j > 1$. We omit this refinement as outside the scope of our investigation, although possibly deserving of further examination elsewhere. We retain the second term in brackets in succeeding equations but omit it in calculations for air.

It is expedient to bring the coefficient E into the innermost energy derivative which then operates on the product Ef. Doing so creates an additional first energy derivative of f which can then be combined with the heating term. Combining the heating and diffusion terms in this way yields the result

$$\frac{2q^2\varepsilon^2}{3m} \frac{\partial}{\partial E} \left[\frac{1}{v(E)} \frac{\partial}{\partial E} [Ef(E,t)] - \frac{3q^2\varepsilon^2}{10m[v(E)]^3} \frac{\partial}{\partial E} f(E,t) \right]$$
$$- \frac{q^2\varepsilon^2}{m} \frac{\partial}{\partial E} \left[\frac{f(E,t)}{v(E)} \right]. \tag{44}$$

Using the same approach that was used for scattering by the electric field, we can also write in-scatter and out-scatter transport terms for collision scattering of electrons due to elastic and inelastic cross-sections. We retain the collision integral formulation instead of derived diffusion and heating differential terms. Inelastic scattering is not reducible to these differential forms because of large energy losses that may occur in a single inelastic scatter, preventing the limit $\Delta E \to 0$ from being taken without approximation. Although the differential approximation is valid for elastic scattering because the average energy gain or loss per collision is much smaller than ΔE, it is convenient to treat both elastic and inelastic scattering in the same way.

The complete energy diffusion equation, including a term for gain of electrons (from avalanching, ion pair creation, etc.) and loss of electrons (to attachment), is

$$\frac{\partial f}{\partial t} - \frac{2q^2\varepsilon^2}{3m} \frac{\partial}{\partial E} \left[\frac{1}{v}(E) \frac{\partial}{\partial E} [Ef(E,t)] - \frac{3q^2\varepsilon^2}{10m[v(E)]^3} \frac{\partial}{\partial E} f(E,t) \right]$$
$$+ \frac{q^2\varepsilon^2}{m} \frac{\partial}{\partial E} \left[\frac{f(E,t)}{v(E)} \right] = \tag{45}$$

$$S(t,E) + \rho \int_{E'=0}^{E'=\infty} u(E')f(E')\sigma(E',E)\,dE' - \rho u(E)f \int_{E'=0}^{E'=\infty} \sigma(E,E')\,dE',$$

where

$S(t,E)$ = sources and sinks for electrons of energy E at time t,

$\sigma(E',E)$ = cross-section to scatter electron with incident energy E' into scattered energy E,

$\sigma(E,E')$ = cross-section to scatter electron with incident energy E into scattered energy E'.

11

The second term on the left hand side of equation (45) describes diffusion due to collisions in a uniform electric field. The third term describes the convection of electrons from a lower energy to a higher energy due to the heating effects of drifting through a uniform electric field. The right hand side describes electron sources and sinks, and collision processes between the electrons and the neutral gas molecules. The first integral accounts for electrons scattered from other energies E' into energy E ("in-scatters"). The second integral accounts for electrons scattered from incident energy E to other energies E' ("out-scatters"). The term $S(t,E)$ may include processes proportional to f and processes independent of f.

In this investigation it has been assumed that the ionization density of the air plasma is low enough that only collisions between electrons and neutral molecules need be considered. Thus, electron-electron and electron-ion collisions are excluded from the simple model. We also neglect small-angle Coulomb scattering.

Collisions that must be included are elastic collisions and several kinds of inelastic collisions such as excitation of rotational modes, vibrational modes, and excited states of the target molecule, and ionization of the molecule (ejection of an orbital electron). When used, air composition will be taken to be oxygen and nitrogen in the usual proportions, although other constituents (water vapor, argon) may be considered later.

2.2 Finite Mesh Model of the Energy Diffusion Equation

We can solve integro-differential equation (45) for energy diffusion by defining a finite energy mesh $E_i, i = 1, 2, \ldots, M$ over a suitable domain from zero to some large energy that includes all electrons of interest. (The shorter term *finite mesh* will be used for the finite, bounded mesh of energies so defined.) Time and energy derivatives are approximated by finite differences, and integrals are approximated by finite sums. There are several finite-difference approximations to the differential part of the energy diffusion equation, with varying stability and accuracy properties. We select the Dufort-Frankel scheme[6] because it is inherently stable and simple to implement in matrix operations on a computer. Using this scheme, the differential terms of the energy diffusion equation become

[6] Carnahan, B., H. A. Luther, and J. O. Wilkes, *Applied Numerical Methods*, John Wiley and Sons, New York (1969), p 451.

$$\frac{\partial f}{\partial t} - \frac{2q^2\varepsilon^2}{3m}\frac{\partial}{\partial E}\left[\frac{1}{v}(E)\frac{\partial}{\partial E}[Ef(E,t)] - \frac{3q^2\varepsilon^2}{10m[v(E)]^3}\frac{\partial}{\partial E}f(E,t)\right]$$

$$+ \frac{q^2\varepsilon^2}{m}\frac{\partial}{\partial E}\left[\frac{f(E,t)}{v(E)}\right]$$

$$\simeq \frac{1}{2\Delta t}[f(t+\Delta t,E) - f(t-\Delta t,E)]$$

$$- \frac{2q^2\varepsilon^2}{3m(\Delta E)^2}\left\{\frac{[E+\Delta E]f(t,E+\Delta E)}{v(E+\Delta E/2)} - \frac{2Ef(t,E)}{v(E)} + \frac{[E-\Delta E]f(t,E-\Delta E)}{v(E-\Delta E/2)}\right\}$$

$$+ \frac{q^4\varepsilon^4}{5m^2(\Delta E)^2}\left\{\frac{f(t,E+\Delta E)}{[v(E+\Delta E/2)]^3} - \frac{2f(t,E)}{[v(E)]^3} + \frac{f(t,E-\Delta E)}{[v(E-\Delta E/2)]^3}\right\}$$

$$+ \frac{q^2\varepsilon^2}{2m\Delta E}\left\{\frac{f(t,E+\Delta E)}{v(E+\Delta E)} - \frac{f(t,E-\Delta E)}{v(E-\Delta E)}\right\}. \tag{46}$$

The complete finite mesh model of the energy diffusion equation is

$$\frac{1}{\Delta t}[f(t+\Delta t,E) - f(t-\Delta t,E)]$$

$$- \frac{2q^2\varepsilon^2}{3m(\Delta E)^2}\left\{\frac{[E+\Delta E]f(t,E+\Delta E)}{v(E+\Delta E/2)} - \frac{2Ef(t,E)}{v(E)} + \frac{[E-\Delta E]f(t,E-\Delta E)}{v(E-\Delta E/2)}\right\}$$

$$+ \frac{q^4\varepsilon^4}{5m^2(\Delta E)^2}\left\{\frac{f(t,E+\Delta E)}{[v(E+\Delta E/2)]^3} - \frac{2f(t,E)}{[v(E)]^3} + \frac{f(t,E-\Delta E)}{[v(E-\Delta E/2)]^3}\right\}$$

$$+ \frac{q^2\varepsilon^2}{2m\Delta E}\left\{\frac{f(t,E+\Delta E)}{v(E+\Delta E)} - \frac{f(t,E-\Delta E)}{v(E-\Delta E)}\right\}$$

$$= S(t,E) + \rho\sum_{\substack{j\neq i\\j=1}}^{M} u_j f(t,E_j)\sigma(E_j,E_i) - \rho u_i f(t,E_i)\sum_{\substack{j\neq i\\j=1}}^{M}\sigma(E_i,E_j). \tag{47}$$

One may carry the sums over the range from $j = 1$ to M without exception at $j = i$, because the $j = i$ terms from each sum cancel each other. But the notation used above is clearer.

The last equation can be written in matrix notation as

$$f_i(t+\Delta t) = f_i(t-\Delta t) + \sum_{j=1}^{M} A_{ji} f_j(t) + S_0(E_i,t) \tag{48}$$

where

$$f_i(t) = f(t,E_i),$$

A_{ji} = sum of homogeneous terms for collision, heating, diffusion, and sources/sinks, and where j and i are the column and row indices, respectively,

$S_0(E_i,t)$ = inhomogeneous sources and sinks independent of f (such as ion pair creation by radiation).

The matrix elements A_{ji} must fulfill certain requirements such as conservation of mass, boundary conditions, and numerical stability. To conserve

mass, it is necessary that all electrons leaving an energy level arrive at other energy levels, or

$$\sum_{i=1}^{M} A_{ji} = 0 \tag{49}$$

for every column i, assuming equally spaced energy levels. The difference terms in equation (47) are not necessarily mass-conservative as presented, but calculating A_{ii} as the negative sum of other off-diagonal column entries assures a mass-conservative system. Certain minor changes to the off-diagonal entries are required to maintain the proper solution when this approach is taken. Also, electron attachment cross-sections must be subtracted from the main diagonal term. For numerical stability (and physical realizability), it is necessary that

$$-1 \le A_{ii} \le 0 \tag{50}$$

or else more electrons are removed from energy level E_i than exist there, and

$$0 \le A_{ji} \le 1, \quad j \ne i \tag{51}$$

or else nonphysical "negative" electron densities are scattered to other energy levels.

Because of an idiosyncrasy of the Dufort-Frankel algorithm, differential error between the initial conditions $f(t - \Delta t), f(t)$ tends to be preserved throughout later time-steps, giving the appearance of two solutions differing by a constant amount. One solution occurs at odd time-steps, and the other solution occurs at even time-steps. Replacing $f(t)$ by

$$[f(t + \Delta t) + f(t - \Delta t)]/2$$

after computation of each new $f(t + \Delta t)$ conveniently unifies the solution.

2.3 Elastic Scattering

To solve the finite mesh equation described above, the convection term requires the electron mobility μ as a function of electron energy, or alternatively the collision volume K as a function of electron energy. Elastic scattering is the most frequent result of collision between conduction electrons and gas molecules, under ordinary circumstances. The dominant effect is to randomize the direction of individual electrons (not the net drift velocity due to ambient electric fields) and, on average, to transfer momentum from the electrons to the gas molecules. It is also possible for electrons to gain or lose small amounts of energy from the random thermal motion of the gas molecules. We assume for our model of elastic scattering that the gas is monatomic and has an isotropic Maxwellian distribution of velocities, a model adequate for our purposes. The effective elastic collision cross-section for electrons in such a gas is equal to the elastic collision cross-section for a gas without molecular motion, to a high degree of approximation, when the electrons have an energy $\gg 0.01\ T$ where T is the gas temperature[7] [p 73].

---

[7] Carter, L. L., and E. D. Cashwell, *Particle-Transport Simulation with the Monte Carlo Method*, USAERDA Publication TID-26607, USAERDA Technical Information Center, Oak Ridge, TN (1975), p 73.

We define for each incident electron energy E_i an effective scattering cross-section $\bar{\sigma}(E_i,E_j)$ which is nonzero for $j = i - 1, i, i + 1$ and is zero for all other j. Following a similar approach to that used for scattering by the electric field, we impose constraints to conserve the first and second energy moments. (The zeroth energy moment does not need special treatment.) Let the incident energy E_i be E_b and the energies E_j be E_a, E_b, and E_c (for nonzero $\bar{\sigma}$) where $E_a = E_b - \Delta E$ and $E_c = E_b + \Delta E$. Electrons which scatter from E_b to E_b do not require any cross-section, so we set $\bar{\sigma}(E_b,E_b) = 0$. We require that the effective cross-section be self-adjoint, which is clearly true for elastic scattering. The constraints may then be written

$$(E_a - E_b)\bar{\sigma}(E_a,E_b) + (E_c - E_b)\bar{\sigma}(E_c,E_b) = \int_0^\infty (E' - E_b)\sigma(E', E_b)u' \, dE', \quad (52)$$

$$(E_a - E_b)^2\bar{\sigma}(E_a,E_b) + (E_c - E_b)^2\bar{\sigma}(E_c,E_b) = \int_0^\infty (E' - E_b)^2\sigma(E', E_b)u' \, dE'. \quad (53)$$

Let the first integral be I_1 and the second integral be I_2. Suppose the total elastic scattering cross-section (inversely proportional to elastic collision frequency) is independent of electron energy. This is often the case for electron energies near the gas thermal energy, where electron mobility is essentially independent of ambient electric field. Then

$$I_1 = \int \sigma_0^s(E_b) \, u'(E' - E_b) f_M(E',E) \, dE' \quad (54)$$

where

$f_M(E',E) \, dE'$ = self-adjoint probability of scattering from energy E' into energy E,

$\sigma_0^s(E)$ = total elastic scattering cross-section for incident electrons having energy E.

It can be shown from a hard sphere scattering model that free electrons colliding with molecules in a monatomic gas will have a scattered speed (magnitude of velocity)

$$u' = u - u\xi \frac{m}{M + m} + 2U\zeta\sqrt{\xi} \, \frac{M}{M + m} \quad (55)$$

where M and U are the molecular mass and speed, $m, u,$ and u' are the electron mass, incident speed, and scattered speed, ζ is the direction cosine of the molecular motion relative to the bisector of the incident and scattered electron velocity, and $\xi = (1 + \mu_{scat})/2$, and where μ_{scat} is the cosine of the electron scattering angle.

We use the unitless expression

$$f_M(E',E) \, dE' = \frac{4}{\pi} \sqrt{1 - (2\xi - 1)^2} \, d\xi \, d\zeta f_M(U) \, dU \quad (56)$$

where the probability of the target molecule having speed U is' [p 72]

$$f_M(U) \, dU = \frac{2}{\sqrt{\pi}} \, \beta^3 U^2 e^{-\beta^2 U^2} dU, \quad (57)$$

and where

$$\beta = \sqrt{M/(2kT)} \, ,$$

k = Boltzmann's constant.

Omitting details of the integration, we obtain after discarding small terms

$$I_1 \simeq u\sigma_0^s(E_b)\,(2kT - E)\frac{m}{M}\,, \tag{58}$$

$$I_2 \simeq 2u\sigma_0^s(E)EkT\frac{m}{M}\,. \tag{59}$$

These results are based on the assumption of energy-independent elastic scattering cross-section. If the elastic scattering cross-section is not independent of electron energy, then the transport integral must be evaluated more carefully. Nitrogen is subject to the Ramsauer-Townsend effect and has an anomalously small elastic scattering cross-section at low energies which varies substantially, leading to inaccurate energy distributions through the use of equation (54). The error for oxygen is less pronounced because of lesser variation of the elastic scattering cross-section. As the development of a solution to the energy diffusion equation is of secondary importance in this work, we do not reduce the transport integral for the case of varying elastic cross-section but merely point out the desirability of doing so for the case of air.

We can now solve

$$(E_a - E_b)\,\bar\sigma(E_b,E_a) + (E_c - E_b)\,\bar\sigma(E_b,E_c) = I_1 \tag{60}$$

$$(E_a - E_b)^2\,\bar\sigma(E_b,E_a) + (E_c - E_b)^2\,\bar\sigma(E_b,E_c) = I_2 \tag{61}$$

for $\bar\sigma(E_b, E_a)$ and $\bar\sigma(E_b, E_c)$ using $E_a = E_b - \Delta E$ and $E_c = E_b + \Delta E$.

It can be seen from the results for I_1 that the elastic cross-section tends to scatter hot electrons (relative to the gas temperature) to lower energies and cold electrons to higher energies, as expected, until the median electron energy equals twice the gas average temperature kT and the mean electron energy equals $\frac{3}{2}kT$, assuming zero ambient electric field. More than two effective cross-sections for elastic scattering are not needed, because the energy mesh width ΔE is much larger than the average energy change per collision.

We have incorporated these effective elastic collision cross-sections into the finite energy mesh equation described above, approximating the derivative terms

$$\rho I_1\,\frac{\partial f}{\partial E}\quad\text{and}\quad \tfrac{1}{2}\rho I_2\,\frac{\partial^2 f}{\partial E^2}\,.$$

For zero ambient electric field, the electron energy distribution relaxes with time toward a Maxwellian distribution of energies, as expected, whose average temperature closely matches the gas temperature. Truncation error due to using an energy mesh spacing $\Delta E = 0.1\,kT$ and only 60 energies in the energy mesh leads to small errors of about 1 percent in the final electron temperature and 0.5 percent in the final energy distribution. Reducing the energy mesh spacing to $\Delta E = 0.05\,kT$ and using 120 energies in the energy mesh reduces these errors by a factor of four in each case, suggesting accuracy to second order in the finite mesh equation. The smaller choice of ΔE requires a smaller Δt for stability.

For isotropic elastic scattering, it can be shown that the total elastic scattering cross-section $\sigma_0^s(E)$ is equal to the momentum exchange cross-section

Q_m. Consideration of anisotropic elastic scatters in nitrogen leads to changes not greater than 1 percent,[4] which we shall neglect. We use the recent tabulations of Q_0^0 (total elastic cross-section) for N_2 by Phelps and Pitchford[8] and of Q_m (momentum exchange cross-section) for O_2 by Phelps[9] to define $\sigma_0(E)$, in these gases and in air composed of 79-percent N_2 and 21-percent O_2 by volume.

2.4 Unequally Spaced Energy Mesh

Up to this point, the energy mesh E_i has been tacitly assumed to be equispaced; however this condition can be relaxed. It is helpful to gradually increase the energy mesh spacing as energy increases, so that fewer mesh points are needed. A coarser mesh at higher energies also reduces the effective cross-section where it is largest, thereby permitting a larger time-step to be used. The computation of the effective cross-sections for elastic scattering is only slightly changed with unequally spaced E_a, E_b, and E_c . We also multiply

$$\bar{\sigma}(E_b, E_c) \text{ by } \frac{2(E_c - E_b)}{E_c - E_a} \text{ and } \bar{\sigma}(E_b, E_a) \text{ by } \frac{2(E_b - E_a)}{E_c - E_a}$$

to account for unequal energy mesh spacing.

Central differences taken at E_i for the convection term and the diffusion term become uncentered when an unequally spaced energy is used. Experience shows that uncentering these terms by about 1 percent of ΔE does not introduce important error to the solution. If necessary the convection term can be represented with a three-point quadratic expression to properly center the difference. To account for unequal energy mesh spacing, we multiply the convection term effective cross-section by the factors used for elastic scattering. We multiply the diffusion term effective cross-section by the squares of the same factors.

We use the following recursion to construct an unequally spaced energy mesh, where we first select $\Delta E_0 = 0.05kT$ and $\kappa = 1.01$, for example:

$$E_0 = 0 \tag{62a}$$
$$E_i = E_{i-1} + \Delta E_{i-1} \tag{62b}$$
$$\Delta E_i = \kappa \Delta E_{i-1} \tag{62c}$$

so that

$$\Delta E_i = \kappa^i \Delta E_0 \tag{63}$$

$$E_i = \Delta E_0 \frac{\kappa^i - 1}{\kappa - 1} . \tag{64}$$

This works quite well at all energies. At low energies the spacing is nearly ΔE_0, and at high energies the spacing is nearly $(\kappa - 1)E$. For zero electric field, the error in the energy distribution function at the high end of the en-

[8] Phelps, A. V., and L. C. Pitchford, Anisotropic Scattering of Electrons by N_2 and its Effects on Electron Transport: Tabulations of Cross Section and Results, JILA Information Center Report No. 26, University of Colorado, Boulder, CO (1 May 1985), p 14.

[9] Phelps, A. V., Tabulations of Collision Cross Sections and Calculated Transport and Reaction Coefficients for Electron Collisions with O_2, JILA Information Center Report No. 28, University of Colorado, Boulder, CO (1 September 1985), p 10.

ergy mesh is less than 1 percent for the mesh constants selected, until the distribution is reduced in amplitude by over 10 decades at the high-energy end of the mesh.

For inelastic scattering, variable energy mesh spacing can lead to systematic error and therefore must be used with caution. We have tried several ways of correcting the effective inelastic cross-sections to account for variable energy mesh spacing without complete success. As a minimum correction, the effective cross-sections for inelastic scattering are divided by κ. For example, results for the energy distribution are low by about 15 percent for energies above several electron-volts, using $\kappa = 1.01$, because of dominance by rapidly changing inelastic cross-sections at energies of several electron-volts. We must use a variable-spaced mesh when covering thermal energies to ionizing energies (above roughly 14 eV) because approximately 10,000 equispaced energies would be needed. Dense matrices of such size are too large for available computers.

2.5 Exact Solutions and Equilibrium Finite Mesh Solutions Compared

Exact solutions for the equilibrium electron energy distribution are known[1] [pp 71-75] when scattering is limited to elastic scattering and (1) electron drift velocity is much less than the mean molecular speed (Maxwellian distribution) or (2) electron drift velocity is much greater than the mean molecular speed and the elastic cross-section is independent of energy (Druyvesteyn distribution). In the first case the time between collisions (reciprocal of collision frequency) is independent of electron energy; in the second case the pathlength between collisions (or collision cross-section) is independent of energy.

For zero ambient electric field, the Maxwellian distribution of electron energies is

$$f(E) = Ae^{-E/kT}. \tag{65}$$

For large ambient electric field, the Druyvesteyn distribution of electron energies is

$$f(E) = A\sqrt{E} \, \exp\left(-\frac{3m}{M} \left[\frac{NQ_m}{q\varepsilon} \right]^2 E^2 \right) \tag{66}$$

where q_m is independent of electron energy.

It is easy to show that the energy mesh equation (eq (47)) correctly models these distributions by applying the principle of detailed balance to the energy distribution function. For our case of a tridiagonal transition matrix where transitions only occur between adjacent energies, detailed balance states that in the equilibrium limit the rate of electrons going from energy E to energy $E + \Delta E$ equals the rate of electrons going from energy $E + \Delta E$ to energy E. Assume an equispaced energy mesh. Define the rate of upgoing electrons as $R^+(E)f(E)$ and the rate of downgoing electrons as $R^-(E + \Delta E)f(E + \Delta E)$. Then detailed balance gives

$$\frac{f(E)}{f(E + \Delta E)} = \frac{R^-(E + \Delta E)}{R^+(E)}. \tag{67}$$

Take the case of the Maxwellian distribution, where $\varepsilon = 0$ and therefore $J_1 = J_2 = 0$. From previous derivations, we have

18

$$R^+(E) = \frac{1}{2(\Delta E)^2}(I_2 + I_1\Delta E) \qquad (68a)$$

$$R^-(E + \Delta E) = \frac{1}{2(\Delta E)^2}(I'_2 - I'_1\Delta E) \qquad (68b)$$

where the primed quantities are evaluated at $E + \Delta E$ and the corresponding unprimed quantities are evaluated at E. Then

$$\frac{R(E + \Delta E)}{R(E)} = \frac{(I'_2 - I'_1\Delta E)}{(I_2 + I_1\Delta E)} . \qquad (69)$$

Assuming $\sigma_0^i(E) = \varsigma/u(E)$ where ς is independent of energy, and dropping second and higher powers of ΔE, we obtain after some manipulation

$$R^-(E + \Delta E)/R^+(E) \simeq \frac{1 + \dfrac{\Delta E}{2kT} + \dfrac{\Delta E}{2E}}{1 - \dfrac{\Delta E}{2kT} + \dfrac{\Delta E}{E}} \qquad (70)$$

which equals, to the order of ΔE retained, the exact solution

$$\frac{e^{\Delta E/kT}}{\sqrt{1 + \dfrac{\Delta E}{E}}} . \qquad (71)$$

Similarly, for high electric fields such that $kT \ll E$, and also neglecting the high-order correction diffusion term, the downscatter and upscatter transition rates between energy levels $E + \Delta E$ and E are

$$R^-(E + \Delta E)f(E + \Delta E) = \frac{2q^2\varepsilon^2}{3m(\Delta E)^2}\frac{[E + \Delta E]f(E + \Delta E)}{v(E + \Delta E/2)}$$
$$- \frac{q^2\varepsilon^2}{2m\Delta E}\frac{f(E + \Delta E)}{v(E + \Delta E)} - \frac{m\rho u\sigma_0^s\Delta E}{2M(\Delta E)^2}f(E + \Delta E) \qquad (72a)$$

and

$$R(E)f(E) = \frac{2q^2\varepsilon^2}{3m(\Delta E)^2}\frac{Ef(E)}{v(E)} + \frac{q^2\varepsilon^2}{2m\Delta E}\frac{f(E)}{v(E)} + \frac{m\rho u\sigma_0^s\Delta E}{2M(\Delta E)^2}f(E) \qquad (72b)$$

where terms involving kT have been neglected. We now apply equation (67). Using $m\sigma_0^i = Q_m$ and $v = NuQ_m$, after some manipulation we arrive at

$$\frac{f(E - \Delta E)}{f(E)} = 1 - \frac{\Delta E}{2E} + 2BE\Delta E \qquad (73)$$

where

$$B = \frac{3m}{M}\left(\frac{NQ_m}{q\varepsilon}\right)^2$$

which agrees to first order with the Druyvesteyn distribution

$$f(E) \propto \sqrt{E}\, e^{-BE^2}$$

In order to establish convergence and consistency of our numerical solution to the energy mesh equation (eq (47)), we numerically calculate equilibrium

solutions for the (65) and (66). All elements A_{ji} of matrix $\mathbf{A}$ in equation (48) must be smaller than unity in magnitude for the equation to converge numerically. Otherwise, numerical instabilities occur. The elements on the main diagonal and first upper and lower subdiagonals contain terms proportional to the square of the electric field ε. These terms become very large as the electric field becomes large. The time stepsize, a multiplier of these these terms, must be reduced to very small values to keep the corresponding elements smaller than unity and maintain numerical stability. Solutions for the energy distribution function may take several microseconds to relax toward equilibrium. If the time stepsize is reduced to 1 fs (1 fs = 0.001 ps) to maintain stability, for example, thousands of hours of computer running time will be needed to find an equilibrium solution. However, the number of iterations of the time-advancement algorithm can be reduced drastically by increasing the number of time-steps the energy distribution function is advanced at each iteration. This is done by constructing a single matrix which advances the distribution function vector many time-steps at a single multiplication.

Omit the inhomogeneous term $S_0(E,t)$ from equation (48) and define the notation $f_n \equiv f(n\Delta t)$. Then the equation becomes

$$f_n = f_{n-2} + \mathbf{A}f_{n-1}. \tag{74}$$

The averaging process of f_n and f_{n-2} to reduce differential error in the initial conditions f_1, f_0 becomes

$$f'_{n-1} = \tfrac{1}{2}(f_n + f_{n-2}), \tag{75}$$

where f'_{n-1} is subsequently used in place of f_{n-1}. Assume initial conditions $f'_0 = f_1 = 0$. Then f_n is defined recursively by

$$f_n = \mathbf{A}f_{n-1} + f'_{n-2}, \tag{76}$$

$$f'_{n-1} = \tfrac{1}{2}(f_n + f'_{n-2}). \tag{77}$$

Introduce matrices $\mathbf{B}_n$ and $\mathbf{C}_n$ such that $f_n = \mathbf{B}_n f_0$ and $f'_{n-1} = \mathbf{C}_n f_0$. Recursions for these matrices can easily be derived, based on equations (76) and (77): We can control the growth of numerical roundoff error by normalizing the determinant of matrix $\mathbf{B}$ to unity at each recursion. Thus with the above initial conditions and defining $\mathbf{I}$ = identity matrix, we have the recursion

$$\mathbf{B}_1 = \mathbf{I}, \qquad \mathbf{C}_1 = \mathbf{I},$$

$$\mathbf{B}'_{n+1} = \mathbf{A}\mathbf{B}_n + \mathbf{C}_n, \tag{78}$$

$$\mathbf{B}_{n+1} = \frac{\mathbf{B}'_{n+1}}{\|\mathbf{B}'_{n+1}\|}, \tag{79}$$

$$\mathbf{C}_{n+1} = \tfrac{1}{2}(\mathbf{B}_{n+1} + \mathbf{C}_n). \tag{80}$$

Now that we have $\mathbf{B}_n$ for any n, where $f_n = \mathbf{B}_n f_0$, we can advance from f_n to f_{2n} by using $f_{2n} = \mathbf{B}_n f_n$. This requires only the additional assumption that $f_{n+1} = f_n$, which is a good approximation. The function f will relax toward the equilibrium state for any reasonable choice of initial conditions, and equation (80) will guarantee that differential errors diminish (being roughly halved at each application). Taking $n = 10$, for example, reduces differential error by about a factor of a thousand. Thus, the function f can be advanced
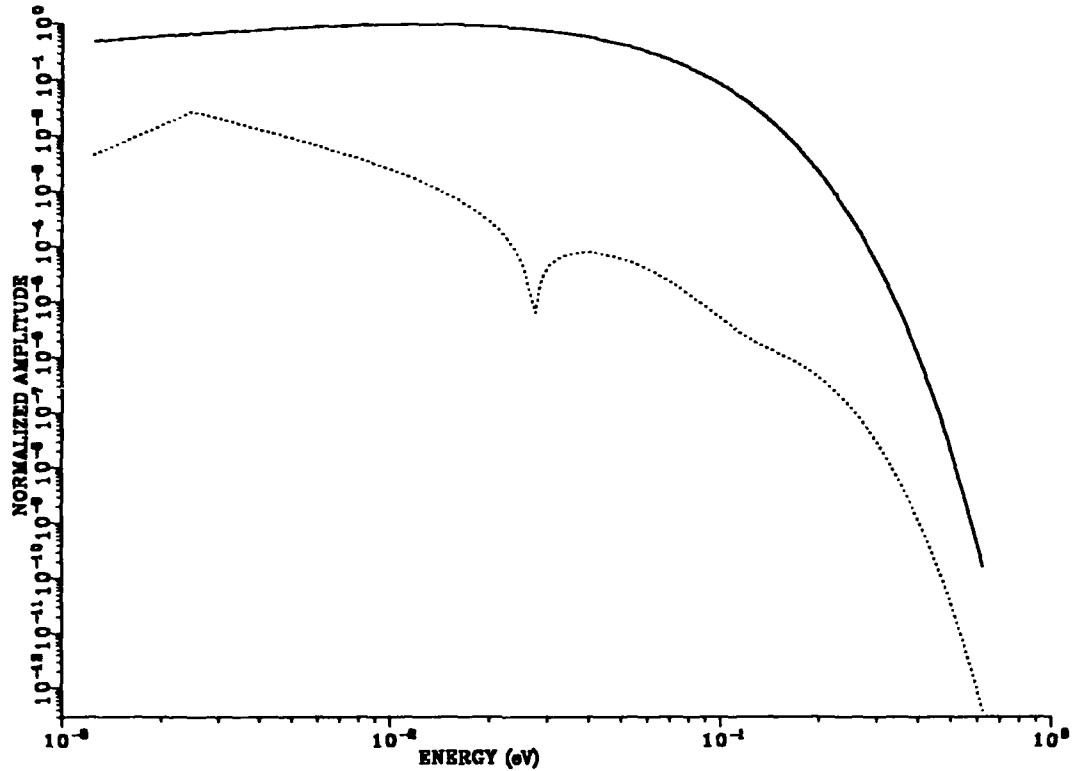
Figure 1. Finite mesh equilibrium results for Maxwellian distribution: Solid line is finite mesh result, dashed line is Maxwellian distribution for electron temperature T such that $kT = 0.025$ eV, and dotted line is magnitude of the difference. The two distributions have been matched at the maxima to eliminate normalization error. Arbitrary units are used for the dependent axis. Only elastic scatters are considered.

in leaps of $2^m \times 10$ time-steps by (1) calculating B_{10} using the above recursion, (2) calculating matrix

$$\mathbf{D}_m \equiv (\mathbf{B}_{10})^{2^m} \tag{81}$$

by using the recursion

$$\mathbf{D}_0 = \mathbf{B}_{10}, \qquad \mathbf{D}_{i+1} = \mathbf{D}_i^2, \tag{82}$$

and (3) multiplying f by $\mathbf{D}_m$ for each leap. For the appropriate choice of m in evaluating matrix $\mathbf{D}_m$, equilibrium solutions can be calculated rapidly even for large values of the electric field. Additionally, an elementary result of linear algebra shows that, as $m \to \infty$, the columns of $\mathbf{D}_m$ each approach the eigenvector $f_\infty = g(E)$ multiplied by a different scalar factor for each column (hence the infrequent usage "eigencolumn" for "eigenvector").

To test the finite mesh equation, we have obtained equilibrium solutions by iterating the time leap (for $n = 10$ and $m = 25$) until the energy distribution became unchanging, for mesh constant $k = 1$ for the Maxwellian case and
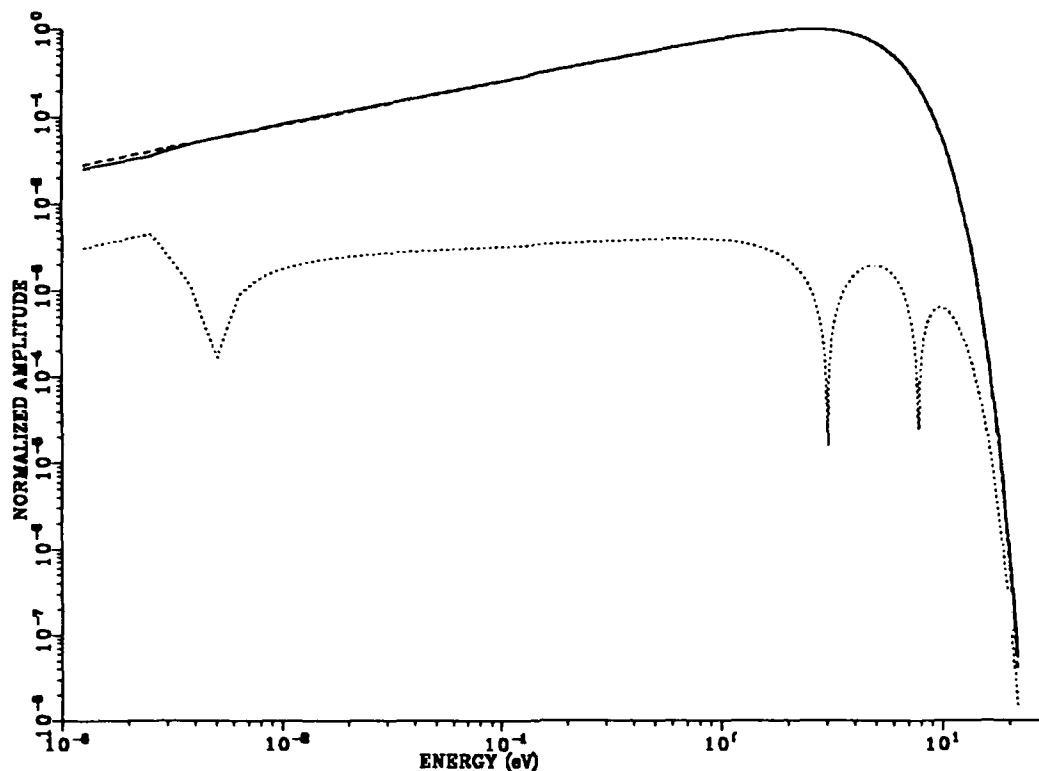
21

Figure 2. Finite mesh equilibrium results for Druyvesteyn distribution: Solid line is finite mesh result, dashed line is Druyvesteyn distribution for electron mean energy equal to 100 times gas thermal energy, where $kT = 0.025$ eV, and dotted line is magnitude of the difference. The two distributions have been matched at the maxima to eliminate normalization error. Arbitrary units are used for the dependent axis. Only elastic scatters are considered.

$k = 1.01$ for the Druyvesteyn case, using $\Delta E_0 = kT/20 = 0.00125$ eV. For the Maxwellian case, the elastic cross-section σ_0^s was made to be constant. For the Druyvesteyn case, σ_0^s was made to vary as $1/u(E)$ except at the lowest energies, where σ_0^s was made nearly constant to avoid the singularity at $E = 0$. Also, the high-order correction diffusion term was neglected. Mean electron temperatures equal to kT (Maxwellian distribution) and $100kT$ (Druyvesteyn distribution) were used. A lower boundary condition was applied which requires $f(E_1) = f(E_2)/\sqrt{2}$. Calculated results for the Maxwellian distribution and error compared to the exact solution are shown in Figure 1 on page 21. Similar results for the Druyvesteyn distribution are shown in Figure 2. As can be seen, the energy mesh equation gives satisfactory results even many orders of magnitude down from the distribution maximum. Noticable error occurs at the lowest energies because of the large spacing of the energy mesh compared to the electron energy.

22

2.6 Inelastic Scattering

Inelastic scatters of incident electrons by gas molecules can involve large changes in energy, in contrast to small changes caused by elastic scattering and scattering by the ambient electric field. For small changes, the zeroth, first, and second energy moments of scattering probability (integrating over the entire energy spectrum) can be represented accurately using distribution function values at only three adjacent energies in the energy mesh. We have shown how such a three-point scheme approximates the sum of a convective first derivative and a diffusive second derivative with the derivatives evaluated at the scattered electron energy, which is equivalent to expanding the energy distribution function to second order in the neighborhood of the scattered electron energy to estimate the "in-scatter" collision integral. To preserve accurately the same first three energy moments of scattering probability when large changes in energy occur, it is necessary to expand the energy distribution function to second order in the neighborhood of the *incident* electron energy. Because the energy change is fixed for each separate excitation/de-excitation process (except for ionization), the integral of the energy moment of the process cross-section reduces to a product. That is, the probability of the electron scattering from E' to E is a delta function, $\delta(E' - E)$. Thus,

$$\int_0^\infty u(E')\sigma_k(E')(E' - E_i)^n \, dE' = (\delta E_k)^n u(E_i + \delta E_k)\sigma(E_i + \delta E_k) \qquad (83)$$

where

$\sigma_k(E) = k$th process cross-section,

$\delta E_k = k$th process energy loss,

$E_i = i$th energy in the energy mesh.

Although the scattered energy will always be a mesh energy E_i, the incident energy will generally lie between two mesh energies E_j and E_{j+1}. The cross-section given for the incident energy must therefore be approximated by equivalent cross-sections at the two mesh energies E_j and E_{j+1}. The equivalent cross-sections are chosen in such a way that, when combined, they conserve the actual cross-section and its first energy moment. Because only two mesh points are used, an error is introduced in second and higher energy moments which diminishes in relative importance for larger energy losses.

For N_2 rotational excitation we use the two-term approximation proposed by Phelps and Pitchford[8] (upper table therein). As explained by Goldstein,[10] this two-term approximation incorporates a continuous scattering term to represent rotational excitation at electron energies less than 0.8 eV and a single-level excitation term with 0.02-eV energy loss to represent rotational excitation near the 2-eV resonance of the N_2 molecule. This two-term approximation was adjusted by its originators to reproduce the diffusion coefficient and mobility parameters for the electron distribution function. The continuous approximation used includes only a first derivative term, instead of first and second derivative terms as recommended by Carron recently,[5] but reproduces the principal transport coefficients in the energy range where rotational excitation is important. It should be pointed out that the collision

[10] Goldstein, B., A Summary of Rotational and Vibrational Cross Sections in N_2, Mission Research Corporation Report MRC-R-1057 (26 January 1987).

operator described by Goldstein (his equation (1), drawn from Frost and Phelps[3]) and also the two-term approximation (his equation (11)) are valid for the steady-state coupled equations that Frost and Phelps obtained by expanding the electron distribution function in a harmonic expansion of Legendre polynomials, and are not the correct collision operators for the time-dependent Boltzmann equation as a function of velocity or energy. For example, the coefficients for inelastic collision terms in Goldstein's expression of the collision operator must be divided by energy loss and multiplied by electron speed to be used with the time-dependent Boltzmann equation described. For O_2 rotational excitation, we use the single-level approximation proposed by Phelps.[9]

Vibrational excitation cross-sections for N_2 are taken from Phelps,[8] which includes tabulations for transitions from ground state ($v' = 0$) to each of the first eight excited states ($v'' = 1$ to 8). Ground state was the only state assumed to be populated among the neutral molecules. Similarly, O_2 cross-section tabulations for transitions from ground state to the first four excited vibrational states were used,[9] including both low-energy and 9-eV resonance data. Electronic excitation and ionization cross-section tabulations were drawn from the same sources.

For rotational, vibrational, and electronic excitation processes, the energy lost by the incident electron is well-defined and fixed for each transition. However, for ionization the residual kinetic energy must be partitioned between the scattered electron, the ejected electron, and a possible excited state of the target molecule. Cross sections for ionization excitation of N_2 are available[11] but are scarce for O_2. Some results are likewise available on the energy distribution of the ejected electron. For the present study, we will simply assume a ground state N_2^+ product and divide the remaining kinetic energy equally between the scattered electron and the ejected electron.

Two-body and three-body attachment cross-sections are used for molecular oxygen.[9] The term "equilibrium energy distribution" in oxygen or air (or other attaching gases) requires special interpretation, because all free electrons ultimately attach. We interpret the equilibrium energy distribution for an attaching gas in the absence of electron sources to be the limit of the energy distribution as the electron density goes to zero. In general, such a limit will exist. When electron sources exist, such as ionization sources or avalanching (breakdown) sources, different interpretations are required. For a constant source of electrons such as time-independent ionizing radiation, the electron density will tend toward a finite limit and the corresponding equilibrium energy distribution will be defined as for nonattaching gases. For an increasing source of electrons through avalanching, gas molecules would ultimately become stripped of electrons and electron density limited. However, we would be more interested in a quasi-equilibrium state where electron density growth is exponential and electron energy has attained some temporarily stationary distribution. This quasi-equilibrium distribution is the interpretation we would use in such a case.

[11] Wadzinski, H. T., and J. R. Jasperse, Low Energy Electron and Photon Cross Sections for O, N_2, and O_2, and Related Data, Air Force Geophysics Laboratory (PHY), Report AFGL-TR-82-0008 (4 January 1982).
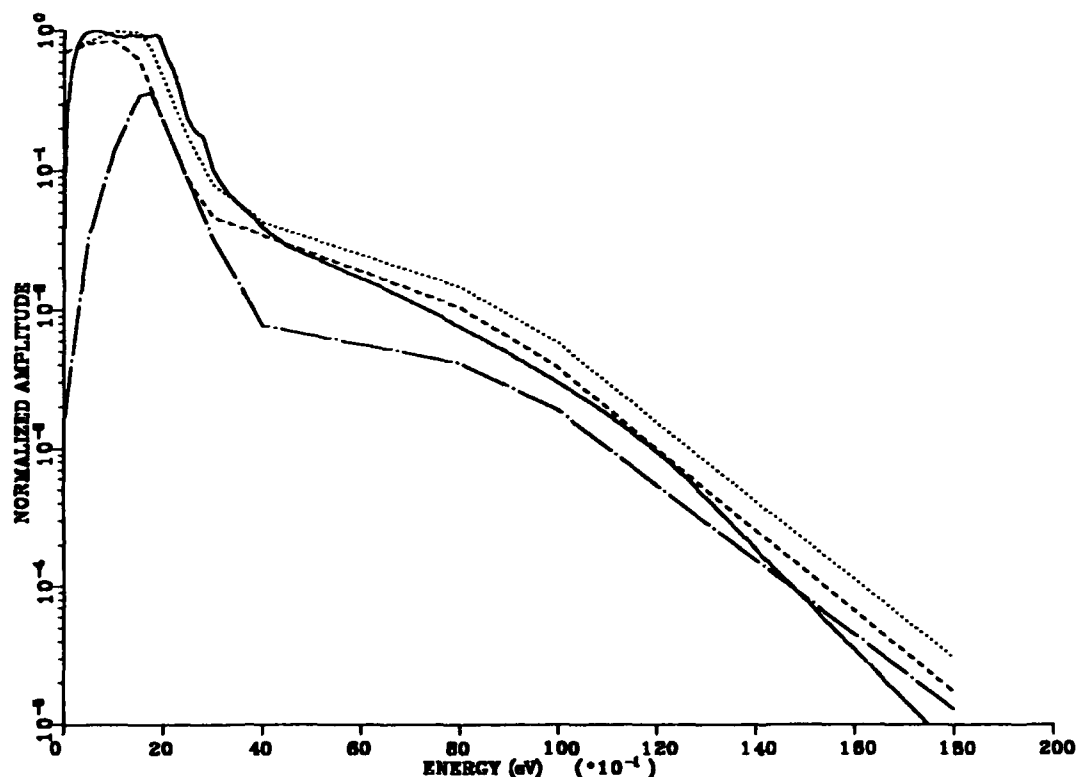
Figure 3. Finite mesh results and first two Legendre coefficients compared: Solid line is finite mesh result, dashed line is first Legendre coefficient of Phelps and Pitchford, dash-dotted line is second Legendre coefficient, and dotted line is sum of two Legendre coefficients. The Legendre coefficients have been normalized so that the maximum of the sum is unity. The maximum of the finite mesh result is also unity. The finite mesh result has been divided by the square root of the energy to conform to the Legendre coefficients. All curves were calculated for $\varepsilon/N = 100$ Td in nitrogen.

2.7 Equilibrium Energy Distribution Compared to Previous Results

Figure 3 compares equilibrium energy spectrum results of the finite mesh equation with our rough digitizations of Phelps and Pitchford's equilibrium energy spectrum[12] for pure molecular nitrogen. The spectra were calculated for $\varepsilon/N = 100$ Td (1 Townsend or Td $= 1 \times 10^{-17}$ V-cm²/molecule) where N is molecular density and ε is electric field strength. The complete set of inelastic cross-sections for N_2 was used for the finite mesh equation. The energy mesh was constructed for $\kappa = 1.015$ and $\Delta E_0 = kT/20$, except that a maximum mesh spacing of $2kT$ was permitted. The finite mesh result is compared with the first two Legendre coefficients of a six-term solution for the electron energy distribution function. The sum of the first two Legendre coefficients

---

[12] Pitchford, L. C., and A. V. Phelps, Comparative calculations of electron-swarm properties in N_2 at moderate E/N values, Phys. Rev. A **25** (1982), 540-554.

25

compares well with the finite mesh equation result. The latter correctly reproduces the "bump" at about 2 eV caused by the second Legendre coefficient. The sharp drop in the finite mesh result at energies near zero agrees with a Monte Carlo calculation done by Phelps and Pitchford, although our drop is steeper. We attribute the small number of electrons near zero energy to the exceptionally small collision cross-section in this energy regime for nitrogen (the well-known Ramsauer-Townsend effect), allowing electrons to accelerate to significantly larger energies in the electric field between collisions. The high-energy tail is smaller for the finite mesh result than for the Phelps and Pitchford distribution, but rough agreement is observed. The average energy of the finite mesh result is 2.0 eV, compared to 2.2 eV for the Phelps and Pitchford distribution. Noticeable error is seen at various energies, however, which underscores the possible importance of a variational method which might reduce errors in the energy distribution to second order in the computation of swarm parameters.

ε/N (Td)	Mesh (eV)	Average energy factor		Drift velocity (m/s)	
		calculated	measured	calculated	measured
0	$\frac{1}{20}kT$	0.77	1.00	0.00	0.00
0.01	$\frac{1}{20}kT$	1.21	---	3.5×10^2	4.0×10^2
0.1	$\frac{1}{20}kT$	4.3	1.8	1.1×10^3	2.5×10^3
0.3	$\frac{1}{20}kT$	6.4	4.8	2.3×10^3	4.0×10^3
0.3	$\frac{2}{3}kT$	6.5	4.8	2.3×10^3	4.0×10^3
1.0	$\frac{2}{3}kT$	13.	12.	4.6×10^3	5.0×10^3
10.	$\frac{2}{3}kT$	28.	36.	2.7×10^4	2.0×10^4
100.	$\frac{2}{3}kT$	63.	72.	1.5×10^5	1.0×10^5

Table 1.   Calculated and Measured Swarm Parameters in Nitrogen Compared: Approximate swarm parameters from measured data and swarm parameters from finite mesh equation. Swarm parameters are averaged over the electron energy distribution. Electron energy factor is average electron energy divided by average molecular energy $\frac{3}{2}kT$.

2.8 Equilibrium Transport Properties Compared to Measured Data

We calculated ensemble (swarm) mobility, drift velocity, and average electron energy in nitrogen for a small number of ε/N values from zero to 100 Td, using equilibrium solutions of the finite mesh equation. Results are shown in Table 1. Because of significant errors caused by variable energy mesh spacing when used with inelastic cross-sections, two constant mesh spacings were used. A fine mesh ($\Delta E = \frac{1}{20}kT$) was used for ε/N from zero to 0.3 Td, and a coarse mesh ($\Delta E = \frac{2}{3}kT$) was used for ε/N from 0.3 to 100 Td, with an overlap at 0.3 Td. Average electron energy is given in units of $\frac{3}{2}kT$.

Inaccuracy due to energy dependence of the elastic scatter cross-section in nitrogen can be seen, as indicated earlier in the discussion of elastic scattering. The average energy should tend toward unity as the electric field goes to zero, but a different limit is observed. This is strictly due to the energy dependence of the elastic scatter cross-section, as established by additional calculations based on a fixed cross-section. Comparisons with approximate

values taken from published measured data[13] range from poor to good. Accuracy of the approximate values for the data is not more than 10 or 20 percent, given the scatter of data and the difficulty of digitization by inspection of the original graphs. The two finite mesh results at 0.3 Td for the fine and coarse energy meshes agree well with each other. Finite mesh results are in good agreement with data at 1, 10, and 100 Td. Agreement is relatively poor at 0, 0.01, and 0.1 Td because of the varying elastic cross-section.

If our objective were to calculate accurately the swarm parameters directly from the electron energy distribution, we might strive for more accuracy than these results indicate. However, the objective of this work is to demonstrate and evaluate a method which may give good estimates of swarm parameters in the presence of various errors introduced by the cross-section set and by the computation of the electron energy distribution function. Indeed, as will be shown, the method trivially reproduces experimentally determined equilibrium swarm data. The most important test of the method will be calculation of nonequilibrium swarm data, however.

3 Analysis of Equilibrium Projection Method

3.1 Developing the Basis of Equilibrium Energy Distributions

We now desire to construct the basis $\phi(E, \Lambda_i)$ used in equation (6). For convenience, the parameter Λ_i is replaced by the equivalent mapping $\phi(E, \varepsilon_i/N)$, where Λ_i is identified with the density-normalized electric field ε_i in gas having molecular density N. For concreteness, we specify the gas to be air as previously constituted. We restrict the basis to finite values of i, letting i run from 1 to n. The ε_i are chosen so that the corresponding ϕ are nondegenerate and complete in, for example, the finite space $E = E_j$. That is, a suitably bounded function $F(E_j)$ can be approximated as

$$F(E_j) \simeq \sum_{i=1}^{n} p_i \phi(E_j, \varepsilon_i/N), \quad j = 1, \dots, M. \tag{84}$$

This description arises from fitting the continuous function $F(E)$ at the points E_j with a finite sum of linearly independent basis functions $\phi(E_j, \varepsilon_i/N)$ (each multiplied by a coefficient p_i). If $M > n$, the resulting linear system of equations is overdetermined and a solution is obtained typically by minimizing a measure of the error of the approximation. If $M = n$ the system can be solved exactly as

$$F(E_j) = \sum_{i=1}^{n} p_i \phi(E_j, \varepsilon_i/N), \quad j = 1, \dots, n. \tag{85}$$

In our application the functions F and ϕ represent continuous functions of electron energy E. Thus, solving the latter equation so that F is fitted exactly at n energies E_j does not guarantee acceptable behavior of the fit at intervening energies (or energies outside the range of E_j). In that which follows we must be aware that a poor fit at these other energies may drastically alter the calculation of collision volume (for example) for the fitting function

---

[13] Dutton, J., A survey of electron swarm data, J. Phys. Chem. Ref. Data, 4 (1975), 577-856.

shown on the right hand side of equation (85). Conversely, calculating a nonequilibrium collision volume using a measurement of equilibrium collision volume implies knowledge of the distribution at all energies, an implication not consistent with the restriction $M = n$. This means that the use of a measurement of equilibrium collision volume may yield bad results if no consideration is given to the goodness of fit at intervening energies.

A trial basis may be constructed from any set of n distin values of ε_i/N. However, because computations with finite precision will be used, it will be helpful to select values that promote linear independence among equilibrium energy distributions derived therefrom. This can be done, for example, by scattering the values over the range of interest, say, from zero to a selected maximum value. The values may be unequally spaced, if desired.

The coefficients p_i describe the *spectral projection* of $F(E_i)$ onto the ϕ basis and are not uniquely defined while the basis vectors are linearly dependent. In matrix notation with row-column order of subscripts, so that matrix $(\mathbf{R})_{ji} = \phi(E_j, \varepsilon_i/N)$ and vectors $(\mathbf{p})_i = p_i$ and $(\mathbf{f})_j = F(E_j)$, we have

$$\mathbf{f} = \mathbf{R}\mathbf{p}. \tag{86}$$

Each column of matrix $\mathbf{R}$ is a basis vector ϕ for some choice of ε_i/N. Because the collision volume $\hat{K}$ for an ensemble is linearly dependent upon the energy distribution $f(E)$ (see eq (4)), we can write the ensemble total collision volume in the *spectral form*

$$\hat{K}_{total} = \sum_{i=1}^{n} \hat{K}_i p_i \tag{87}$$

where $\hat{K}_i$ is the collision volume for an ensemble whose equilibrium energy distribution corresponds to a choice ε_i/N for electric field divided by molecular density. In matrix notation where $(\mathbf{k})_i = \hat{K}_i$, we write this as

$$\hat{K}_{total} = \mathbf{k}^T\mathbf{p}. \tag{88}$$

Solving equation (86) for $\mathbf{p}$ and substituting in the last equation gives

$$\hat{K}_{total} = \mathbf{k}^T\mathbf{R}^{-1}\mathbf{f}. \tag{89}$$

At this stage, several methods of obtaining unique projection coefficients p_i must be considered. One method is to take $M = n$ and solve equation (85) for the projection coefficients. However, this method is not truly consistent with our desire to obtain a smooth, close fit to the nonequilibrium distribution at intervening energies. Hence we desire to make $M \gg n$ and take account of as many energies as practical. The coefficients p_i may take on positive or negative values as needed to manage the fit at all the E_j, contributing to a numerically unstable solution. Another method is to impose a constraint that $p_i \geq 0$ for each i, and find an approximate solution to equation (86) that satisfies this and perhaps other constraints. Clearly there is no need to settle for an approximate solution if an exact solution is available and usable. Hence we will pursue the exact solution of (86) until it is shown that an exact solution has undesirable properties making it useless. Then we will return to the second, approximate method.

The matrix $\mathbf{R}$ may have a very small determinant (*i. e.*, may be ill-conditioned) in spite of careful choice of ε_i/N, so that its inverse $\mathbf{R}^{-1}$ may be numerically difficult to compute. To avoid computational difficulties of this

kind and to define the p_i uniquely, we transform the trial basis **R** to an orthonormal basis **O** by means of a Gram-Schmidt orthogonalization procedure. Thus we obtain a set of mutually orthogonal basis vectors $\phi'_i(E_j)$ where $j = 1, \dots, M$ using

$$\phi'_1(E_j) = \phi(E_j, \varepsilon_1/N),$$

$$\tilde{\phi}_i(E_j) = \phi(E_j, \varepsilon_i/N) - \sum_{k=1}^{i-1} \phi'_k(E_j) \sum_{l=1}^{M} \phi(E_l, \varepsilon_i/N)\phi'_k(E_l), \quad i = 2, \dots, n$$

$$\phi'_i(E_j) = \frac{\tilde{\phi}_i(E_j)}{\sum_{l=1}^{M} [\tilde{\phi}_i(E_l)]^2}. \tag{90}$$

The vectors can be orthogonalized in any order, but the procedure is described for ascending i without loss of generality. It is assumed that the $\phi(E_j, \varepsilon_i/N)$ are normalized to unity before the production of the ϕ'_i. An improved basis is obtained at each step of the orthogonalization, containing one additional orthogonalized basis vector at each step. The transpose of each improved basis can be represented as the transpose of the previous basis multiplied by a simple lower triangular matrix which has main diagonal terms of unity and no nonzero off-diagonal terms, except for one (ith) row which orthogonalizes the next (ith) basis vector. Thus the transpose of the final, fully orthonormalized basis can be obtained by multiplying the transpose of the trial basis by n lower triangular matrices, or equivalently by one lower triangular matrix which is the product of the n matrices. (The product of lower triangular matrices is also a lower triangular matrix.) In matrix notation, we write the transformation as

$$\mathbf{O}^T = \mathbf{TR}^T \tag{91}$$

where the lower triangular matrix **T** summarizes the Gram-Schmidt procedure. Solving this equation for the inverse of matrix **R** and substituting into equation (89) gives

$$\hat{K}_{total} = \mathbf{k}^T \mathbf{T}^T \mathbf{O}^{-1} \mathbf{f}. \tag{92}$$

By the associative law for matrices, this can be expressed as

$$\hat{K}_{total} = (\mathbf{k}^T \mathbf{T}^T)(\mathbf{O}^{-1}\mathbf{f}), \tag{93}$$

or

$$\hat{K}_{total} = (\mathbf{Tk})^T(\mathbf{O}^{-1}\mathbf{f}). \tag{94}$$

Because matrix **O** is orthogonal its inverse is numerically accessible. The multiplication of the energy distribution function **f** by matrix **O** $^{-1}$ projects the distribution onto the orthonormal basis, which was transformed from the original trial basis of equilibrium distribution functions. The first parenthetical expression likewise transforms the collision volumes belonging to the trial basis into collision volumes belonging to the orthonormal basis.

Note, however, that projecting the energy distribution onto an orthonormal basis does not itself constitute the proposed method of calculating swarm mobility or collision volume. Rather, the essential feature of the proposed method is the identification of the $\hat{K}_i$ in equation (87) (or in eq (9)) as be-
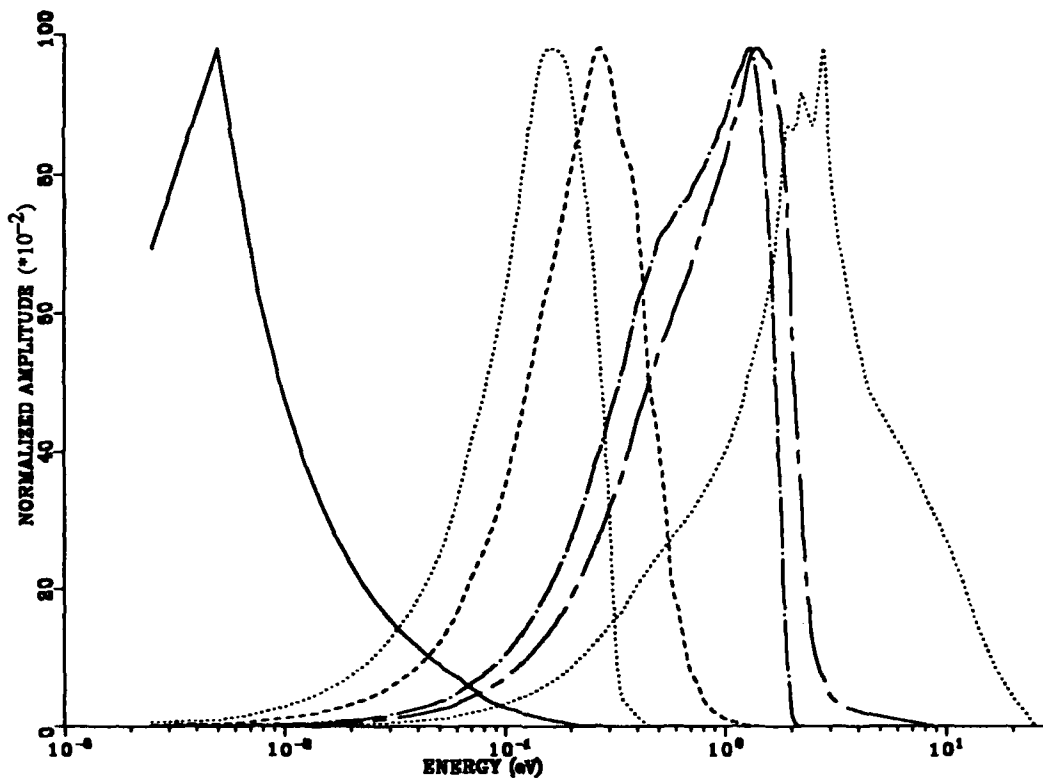
Figure 4. Equilibrium energy distributions as trial basis vectors: Examples of trial basis vectors used for projection onto an equilibrium basis. Equilibrium energy distributions $\phi(E_j, \varepsilon_i/N)$ shown are for $i = 1$ (solid line), 10 (dotted line), 20 (dashed line), 30 (dash-dotted line), 40 (dash-dashed line), and 50 (second dotted line). All curves are normalized to a maximum amplitude of unity.

longing to equilibrium energy distributions $\phi(E_j, \varepsilon_i/N)$ (or $\phi(E, \Lambda_i)$ in eq (6) et seq.). To demonstrate the projection method, we calculated $n = 50$ trial basis functions for air for

$$\varepsilon_i/N = 0.01 \frac{\kappa^{i-1} - 1}{\kappa - 1}, \quad i = 1, \dots, 50 \tag{95}$$

with a choice of $\kappa = 1.2$, which gives a range of values for ε_i/N starting with 0 Td, 0.01 Td, etc., and ending with 379 Td. The finite mesh equation was solved with $M = 550$ mesh points from $\frac{1}{10}kT$ to about 29 eV, to obtain equilibrium energy distributions for the 50 separate values of ε_i/N, using the cross-sections previously discussed for air, except that attachment and avalanching cross-sections were omitted to simplify the calculation. Results were saved on computer disk for later use with the projection method, because of extensive computer time required to calculate the set of 50 distributions. Equilibrium distributions for $i = 1$, 10, 20, 30, 40, and 50 are shown in Figure 4.
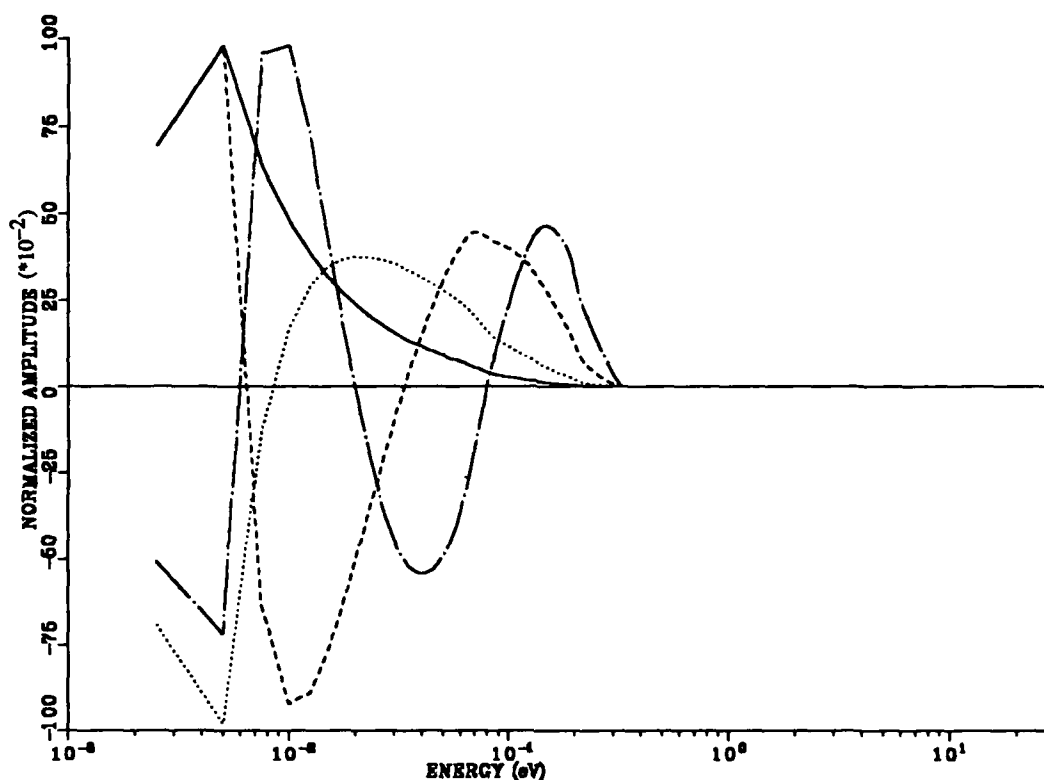
Figure 5. Orthonormal basis vectors derived from equilibrium energy distributions: First four orthonormal basis vectors derived from $\phi(E_j, \varepsilon_i/N)$, $i = 1,2,3,4$. Vectors 1 through 4 are in the order solid, dotted, dashed, and dash-dotted. All curves are normalized to a maximum amplitude of unity.

After these distributions were calculated as the trial basis, an algorithm was applied to orthonormalize the set (using the Gram-Schmidt procedure mentioned) in ascending order of i. As a practical matter, the orthonormalization was accomplished with a weight function proportional to the energy mesh spacing to account for a nonequispaced energy mesh. The first four orthonormal basis vectors so obtained are shown in Figure 5. Typical of orthogonal functions, the number of sign changes increases with the ordinal of the basis vector.

Because M was chosen greater than n, the orthogonalization must incorporate some quantification of the notion of "goodness of fit" which is not needed when $M = n$. This is achieved by selecting the order in which the trial basis vectors are orthogonalized. A good though possibly suboptimal ordering is, at the k th step, to orthogonalize the remaining trial basis vector whose orthogonal form has the largest inner product with the residual nonequilibrium distribution from the previous step $r_j^{(k-1)}$. The residual nonequilibrium distribution at any step is the residual for the previous step less its inner product with the orthogonal form of the trial basis vector selected for orthogonalization at that step:
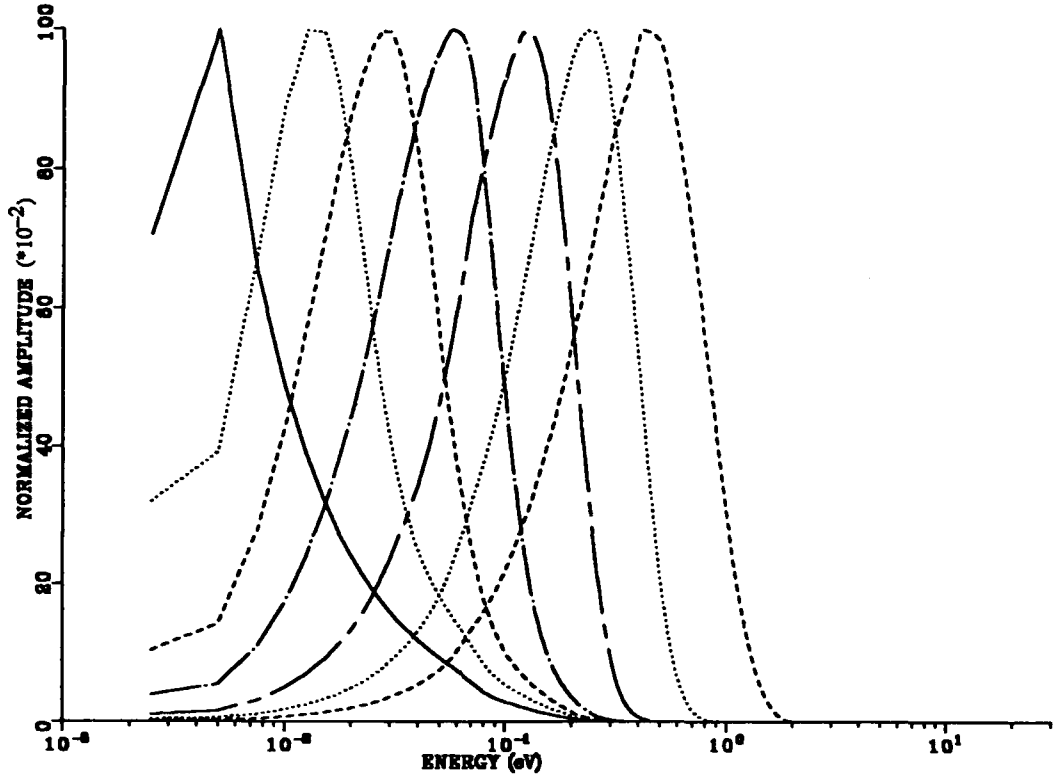
Figure 6. Nonequilibrium energy distributions for step-function electric field: Time-dependent finite mesh equation solutions for a 10-Td step-function electric field, at 0 ps (solid line), 10 ps (dotted line), 50 ps (dashed line), 200 ps (dash-dotted line), 1 ns (dash-dashed line), 4 ns (second dotted line), and 20 ns (second dashed line) after onset of the step function. All curves are normalized to unit amplitude.

$$r_j^{(0)} = F(t, E_j),$$

$$r_j^{(k)} = r_j^{(k-1)} - \phi'_i(E_j) \sum_{l=1}^{n} r_l^{(k-1)} \phi'_i(E_l).$$

As before, the prime notation denotes the orthogonalized form of the basis vector. Thus, at the kth step, we orthogonalize the previously unorthogonalized basis vector $\phi(E_j, \varepsilon_i/N)$ for which the magnitude of the inner product

$$\sum_{l=1}^{n} r_l^{(k-1)} \phi'_i(E_l)$$

is maximized. Selecting the order of orthogonalization in this way requires that a trial orthogonal form be calculated for each vector tested using the inner product. Because any orthogonal form depends on the prior order of orthogonalization, the trial orthogonal form may not be the same as the final orthogonal form calculated for a given basis vector.
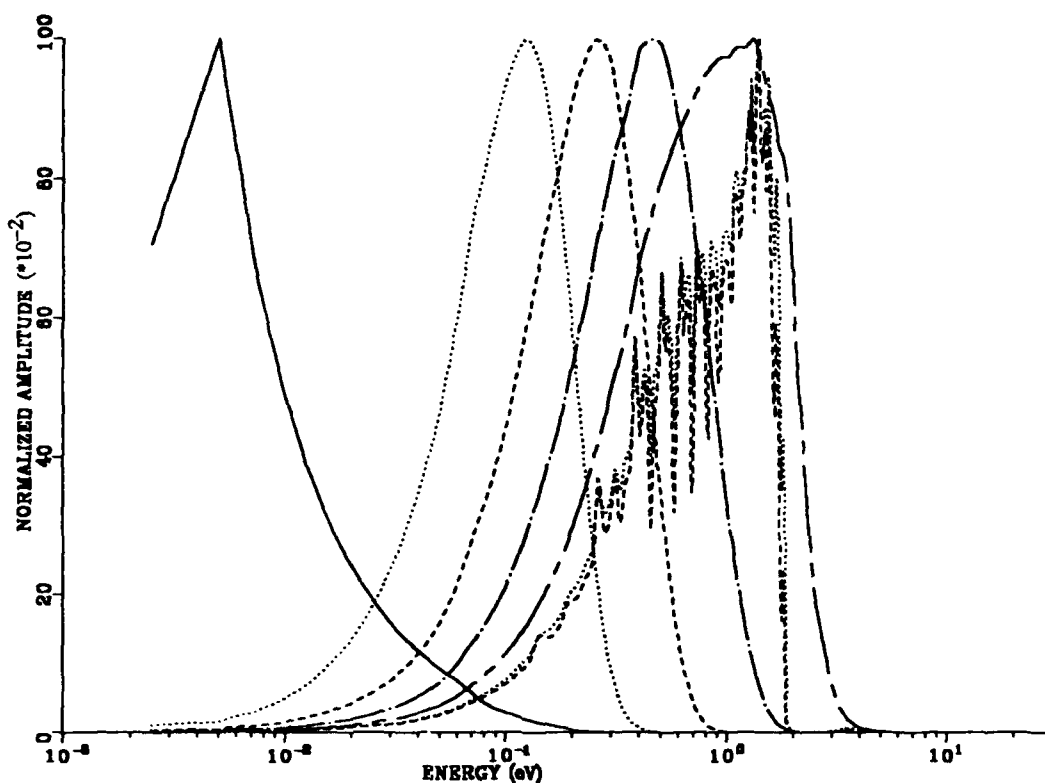
32

Figure 7. Nonequilibrium energy distributions for square-wave electric field: Time-dependent finite mesh
equation solutions for a 100-Td square-wave electric field, at 0 ps (solid line), 10 ps (dotted line), 50
ps (dashed line), 200 ps (dash-dot line), 1 ns (dash-dashed line), 6 ns (second dotted line), and 11 ns
(second dashed line) after onset of the square wave. The square wave lasts 1 ns. All curves are
normalized to unit amplitude.

We used this ordering of the orthogonalization process and the consequent
order of rows of matrix T in the ensuing calculations. The orthogonalization
order (row order of matrix T) may change from one time-step to another,
thereby introducing discontinuities in the calculated collision volume.

3.2 Obtaining Time-Dependent Energy Distributions

To illustrate calculation of time-dependent electron energy distributions, we
select two prescriptions of the ambient electric field: (1) a step increase from
zero field to a constant amplitude of 10 Td, and (2) a square wave of 1-ns
duration and 100-Td amplitude. An air density one-thousandth that at sea
level is selected to reduce the collision rate and emphasize the nonequilib-
rium aspect of the calculation. Using time leaps of 10 ps, we solved the finite
mesh equation for air for both the prescribed electric fields. Initial
(Maxwellian) and subsequent distributions are shown in Figure 6 on page
32 for the first case of a step increase in the field. The figure shows rapid

heating of the electrons on this short time scale, relaxing toward an equilibrium distribution corresponding to a constant electric field-value of 10 Td.

For a short square-wave electric field (shown in Figure 7 on page 33) initial (Maxwellian) and subsequent distributions show the expected maximum heating at 1 ns after the onset of the field, followed by very slow cooling back to the zero field equilibrium. As the distribution cools, the high-energy tail erodes rapidly between 2 and 3 eV, where downscatter cross-sections are greatest for nitrogen. A small island of electrons lingers above 3 eV, where downscatter cross-sections are smaller. A striking feature of the distributions when the electric field has returned to zero is the growth of sharp maxima and minima where specific resonances transfer electrons from one fixed energy to a lower fixed energy. These sharp peaks and valleys occur because the electric field no longer diffuses ("smooths out") the electron energy. Although elastic scattering diffuses electron energy, its effect is much weaker than the effect of the electric field. The presence of a small electric field after the main pulse would keep electron energies well mixed and prevent such an irregular distribution function.

3.2 Projecting Time-Dependent Distributions onto an Equilibrium Basis

The spectral coefficients p_i for projecting $F(t,E_j)$ onto the orthogonalized equilibrium basis $\phi'_i(E_j)$ are plotted for case 1 (step-function electric field) in Figure 8 on page 35 for the same times for which the energy distribution was shown in Figure 6. The spread in the spectrum gives a measure of how far the nonequilibrium energy spectrum has departed from an equilibrium state. The spectral projection is obtained from the equation

$$\mathbf{p} = \mathbf{T}^T \mathbf{O}^{-1} \mathbf{f}. \tag{96}$$

The spectral projection for case 2 (square-wave electric field) is plotted in Figure 9 on page 36. In both figures the dominance of a single equilibrium distribution is observed for every nonequilibrium distribution calculated. Significant additional spectral content occurs for a few cases, primarily the lower energy cases where heating has just begun. At higher energies the dominance of a single equilibrium distribution is more pronounced. The initial (Maxwellian) distribution for zero electric field has a single component at vector ordinal 1, as expected, corresponding to the zero-field equilibrium distribution. At 10, 50, and 200 ps, dominant components at vector ordinals 2 and 3 are seen, with 2 to 4 nearby components of amplitude 10 to 40 percent as great as the dominant component. At later times secondary components appear to contribute less and less, suggesting that the time-dependent distribution is relaxing toward some equilibrium state.

The two distributions occurring 5 and 10 ns after the end of the square-wave electric field are seen to have cooled significantly from the distribution at the end of the electric field pulse, with dominant vector ordinals of 32 and 31 compared to 40 for the latter. These ragged distributions (as shown in Figure 7) are as easily represented by a dominant equilibrium distribution and much smaller secondary components as are the smooth distributions. The convergence of the spectral projection appears rapid regardless of sharp peaks and valleys in the distribution, in these examples.
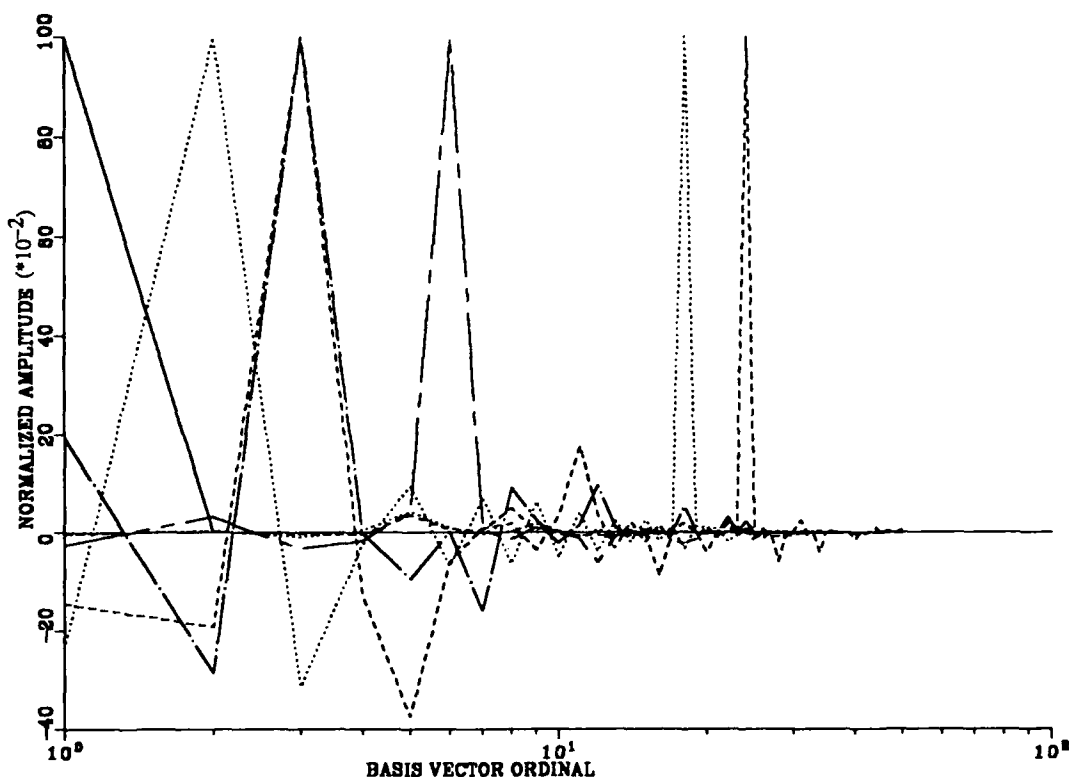
Figure 8. Spectral projections for step-function electric field: Spectral projections of time-dependent finite mesh equation solutions for a 10-Td step-function electric field, at 0 ps (solid line), 10 ps (dotted line), 50 ps (dashed line), 200 ps (dash-dotted line), 1 ns (dash-dashed line), 4 ns (dotted line), and 20 ns (dashed line) after onset of the step function. Abscissa values are ordinal numbers of the orthonormalized equilibrium basis vectors upon which the solutions are projected. A basis is constructed for each solution according to the order of orthogonalization described in the text, so that each basis is different for the solutions shown. However, temperature is a monotonically increasing function of the *dominant* basis vector. All curves are normalized to unit amplitude.

3.3 Defining a Test of the Equilibrium Projection Method

It is important to define carefully what test can be applied to the method of projection onto an equilibrium basis (eq (9)), so that a meaningful comparison can be made with the method of equation (5). If an exact energy distribution is calculable for any equilibrium or nonequilibrium case, depending on the electric field, then the use of equation (5) to evaluate the collision volume is limited only by the accuracy of the momentum exchange cross-section data used. Likewise, the use of equation (9) is limited by the accuracy of the ensemble collision volume data used. (We neglect error arising from discretization of the energy mesh, which in principle can be forced to zero if a sufficiently fine energy mesh is used.) Unfortunately, some experimental error is present in undetermined amounts in both momentum exchange data and ensemble (swarm) collision volume data. We perceive no
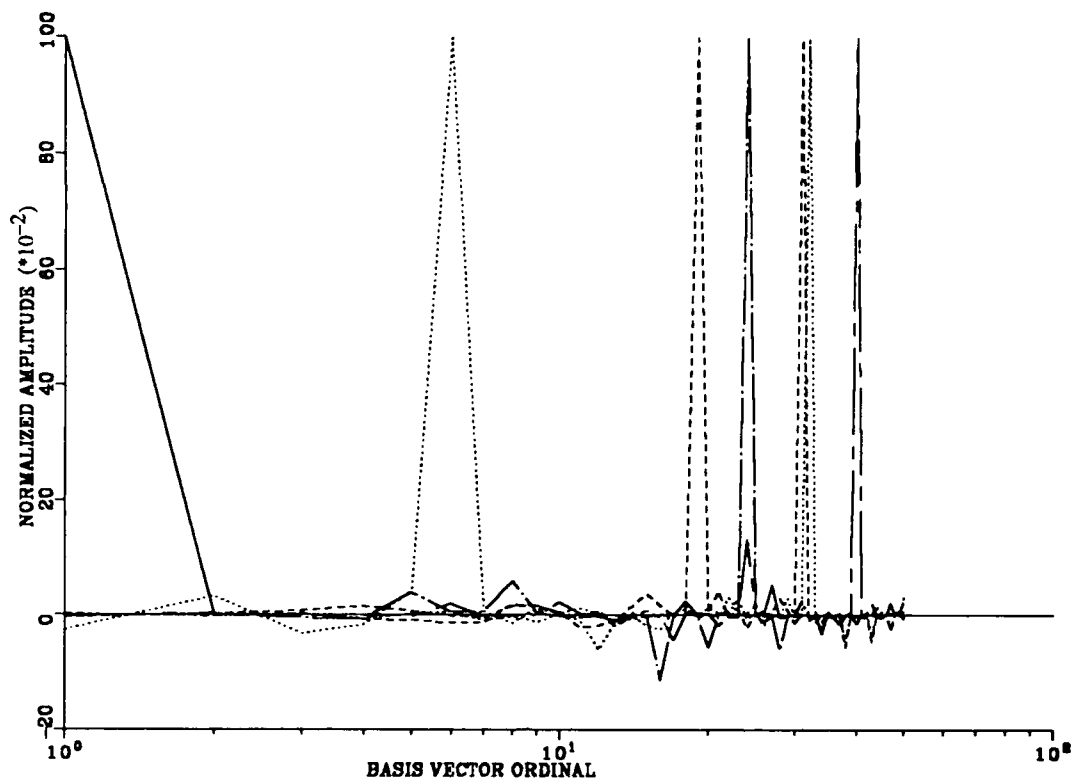
35

Figure 9. Spectral projections for square-wave electric field: Spectral projections of time-dependent finite mesh equation solutions for a 100-Td square-wave electric field of 1-ns duration, at 0 ps (solid line), 10 ps (dotted line), 50 ps (dashed line), 200 ps (dash-dotted line), 1 ns (dash-dashed line), 6 ns (dotted line), and 11 ns (dashed line) after onset of the square wave. Abscissa values are ordinal numbers of the orthonormalized equilibrium basis vectors upon which the solutions are projected. All curves are normalized to unit amplitude.

basis here to say which method is more accurate. The proposed method is not necessarily more convenient because it uses ensemble collision volume data, since computation of the energy distribution function requires use of the momentum exchange cross-section anyway.

On the other hand, equation (9) offers the possibility of variational accuracy in estimates of ensemble collision volume when there are errors in calculation of the energy distribution function and in momentum exchange cross-section data. What is needed to make a comparison, then, is to (1) assume that a baseline set of cross-section data and its derived energy distribution functions are exactly correct, (2) calculate collision volume using either or both methods (results must be the same) from the baseline cross-section data and derived energy distribution functions, to serve as a standard for comparison, (3) introduce "error" to the baseline cross-section data and derive perturbed energy distribution functions, to serve as approximate data, and (4) calculate collision volume using both methods from the approximate data (results will be different) and compare results with the standard ob-

tained in step (2). In this way we can estimate the ability of the proposed method to reduce effects of cross-section error.

The cross-section data used for calculations up to this point will describe the baseline cross-section standard, and equilibrium energy distribution functions obtained using the finite mesh equation will be assumed to be correct for the purposes of the comparison. Ensemble collision volume obtained using equation (4) from these cross-sections and energy distribution functions will describe standard equilibrium collision volumes, assumed to be exactly correct equilibrium values for each electric field strength ε_i/N in the basis.

We define two erroneous cross-section sets incorporating different types of error to test the ability of the proposed method to reduce mobility error due to error in the energy distribution function. In set A every cross-section is twice as large as in the baseline set. This causes an energy scale factor error of a factor of two in the calculated energy distribution function. In set B all rotational cross-sections are twice as large as in the baseline set. This causes a more complex type of error in the calculated energy distribution function.

3.4 Orthogonal Projection Results for a Time-Dependent Distribution

Using the test defined in the previous section, we calculated collision volume for time-dependent energy distributions using cross-section set A. Collision volume was then obtained using the orthonormal projection method described. The orthonormal projection method proved to be generally unsatisfactory, leading to large positive and negative calculated collision volumes for the successive time-dependent energy distributions. Scrutiny of the elements of the orthogonalizing matrix T showed that the maximum size of elements in a row increased sharply as the ordinal of the corresponding basis vector increased. Thus the dominant row maximum was about 10^{12} times larger than the least dominant row maximum. This means that the elements of the least dominant row are very large and of varying sign, leading to very large inner products with collision volume vector k. This is a recognizable consequence of the ill-conditioning of the linear system in equation (86). Although the orthogonalizing matrix T controls error growth in the calculation of matrix O, it exacerbates error growth in the product Tk in equation (94). This is due to the occurrence of both positive and negative row elements in R, T, and O .

It was observed that the spectral form (eq (87)) for an orthonormal projection resembles an asymptotic series at later times when the energy distribution is close to equilibrium. An asymptotic limit is approached for the value of $\hat{K}_{total}$ after a few terms in the expansion (in order from most dominant basis vector to least dominant). Unfortunately this is not the case at intermediate times when the distribution is far from equilibrium.

3.5 Nonnegative Projection Method

A stabler system results from requiring row elements in R to be nonnegative, so that each p_i is nonnegative also. The projection is then approximate, because the exact solution requires no restriction on the sign of elements of R. Such a system may be solved by defining the solution as the minimum of a penalty function which measures the weighted error raised to some power. The penalty function is minimized using a suitable nonlinear optimization procedure, yielding the desired solution for p_i.

We define an approximation to a general energy distribution function $F(E_j)$ as

$$F(E_j) \simeq \sum_{i=1}^{n} \pi_i^2 \phi(E_j, \varepsilon_i/N), \quad j = 1, \dots, M, \tag{97}$$

where the coefficients π_i may be positive or negative, but their squares are obviously nonnegative. Hence the projection (97) is nonnegative. The penalty function is defined as

$$P\{\pi_j\} = w_j^2 \left[F(E_j) - \sum_{i=1}^{n} \pi_i^2 \phi(E_j, \varepsilon_i/N) \right]^2. \tag{98}$$

For any time-dependent energy distribution function $F(E)$, minimization of P over the allowable space of π_j yields a solution for the π_i. The solution may be unique, depending on whether the minimum is global or merely local. We multiply the bracketed term by a weight function w_i to emphasize significant segments of the distribution. For calculation of ensemble collision volume, an appropriate choice of weight function is the collision volume $K(E_j, \varepsilon_i/N)$ raised to the same power as the bracketed quantity. Minimizing such a penalty function yields a weighted least-squares approximation to $F(E_j)$ and a least-squares approximation to the ensemble collision volume.

We have obtained such a nonnegative projection approximation to the energy distribution function, using a conjugate gradient minimization procedure. The projection coefficients obtained were sharply defined in each case, consisting of a few adjacent nonzero components and occasionally a smaller component some distance away. When collision volume was calculated using the spectral form for the baseline cross-section set and erroneous cross-section sets A and B, and compared with results using the conventional method of equation (5), the spectral form gave poor results. We infer that the approximation error was too large to give acceptable results.

The calculation of collision volume is improved by using the approximation error to calculate a residual collision volume using the conventional method, which is then added to the spectral calculation of collision volume. Thus,

$$\hat{K}_{total} = \sum_{i=1}^{n} \hat{K}_i p_i + \sum_{j=1}^{M} \left[F(E_j) - \sum_{i=1}^{n} p_i \phi(E_j, \varepsilon_i/N) \right] K(E_j) \tag{99}$$

describes an approximate projection with "cleanup" of the residual using the method of equation (5). Although improvement was noted, the calculated ensemble collision volume still compared poorly to a conventional calculation. After some study, this was attributed to poor linear independence of adjacent nonzero components in the nonnegative projection. That is, in equation (22) the term $r(E,t)$ is not small compared to $f(E,t)$ for the case under consideration.

As a last resort the nonnegative projection was restricted to a single nonzero component and the residual was "cleaned up." This single-vector projection with "cleanup" is equivalent to (1) finding the equilibrium distribution closest to the nonequilibrium distribution $F(E_j,t)$ (closest in the sense of minimizing the least-square error previous discussed), (2) applying a conventional collision volume calculation to the residual ("cleanup"), and (3) adding to the latter result the ensemble collision volume of the selected equilibrium distribution. The results obtained are shown in Figure 10 on page 39 for the
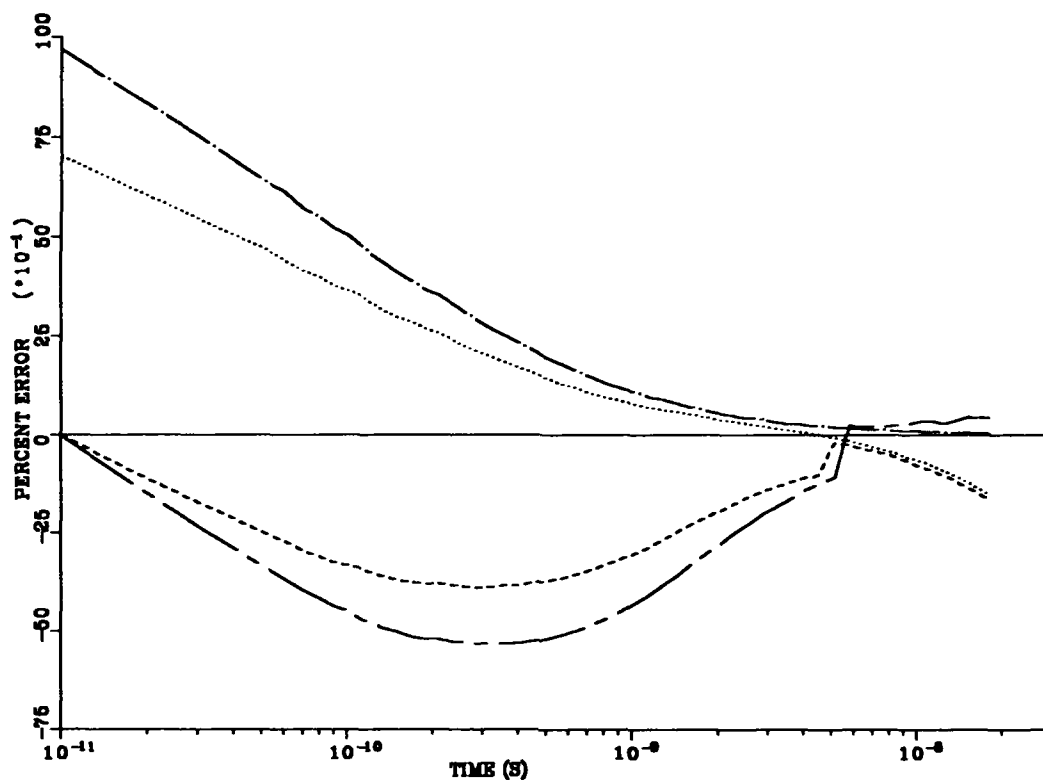
Figure 10. Error in calculated ensemble collision volume for step-function E-field: Plotted error for projection method and conventional method based on various cross-section sets, compared to exact calculation of ensemble collision volume for the case of a square-wave electric field. Dotted line is error for conventional method using Set A. Dashed line is error for projection method using Set A. Dash-dot line is error for conventional method using Set B. Dash-dash line is error for projection method using Set B. Solid line is error for projection method using Baseline Set (exactly zero).

step-function electric field and in Figure 11 on page 40 for the square-wave electric field. These results are the most successful obtained by the equilibrium projection method. For the 10-Td step-function electric field, the projection method sharply reduces error (due to cross-section sets A and B) for the first 100 ps, while the electron energy distribution is close to its initial equilibrium state. As the error in the conventionally calculated collision volume fortuitously passes through zero, the projection method displays more error, and then both methods give nearly equal error at late times. For the 100-Td square-wave electric field, the projection method gives zero error at the initial equilibrium but promptly develops larger error at the next time-step 10 ps later, before converging to nearly the same error as the conventional method at late times.
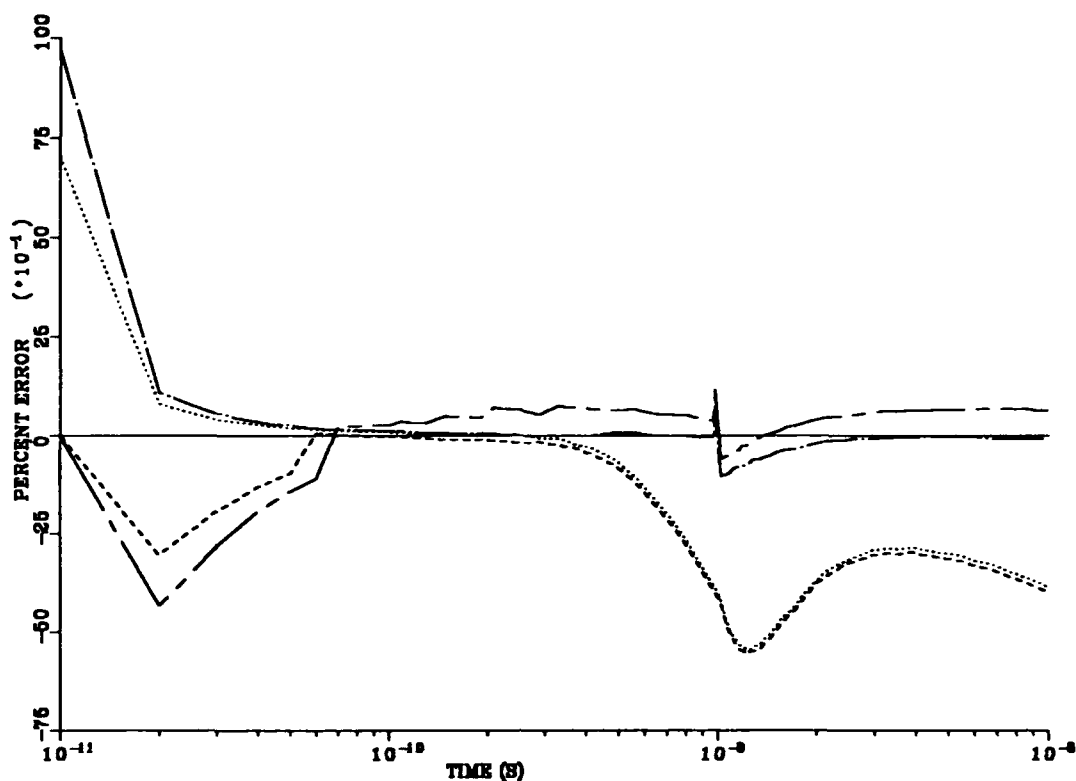
Figure 11. Error in calculated ensemble collision volume for square-wave E-field: Plotted error for projection method and conventional method based on various cross-section sets, compared to exact calculation of ensemble collision volume for the case of a step-function electric field. Dotted line is error for conventional method using Set A. Dashed line is error for projection method using Set A. Dash-dot line is error for conventional method using Set B. Dash-dash line is error for projection method using Set B. Solid line is error for projection method using Baseline Set (exactly zero).

4 Discussion

The use of an orthogonal basis for the projection method was found to create unusable results for the spectral form of $\hat{K}_{total}$ because of the occurrence of very large positive and negative elements of matrix T. This is because of the inherent linear dependence of the basis $\phi(E_j, \varepsilon_i/N)$, and is a fundamental shortcoming of the projection method. If the basis could be restricted to a small number of basis vectors possessing a high degree of linear independence, the projection method might make a better showing in cases not discussed. Figure 4 shows that the equilibrium distributions for $i = 1$ and $i = 50$ are the most nearly linearly independent of those shown, as would be expected. However, it is difficult to find a realistic case which consists of a sum of these two distributions alone. Comparison of the equilibrium distributions of Figure 4 and the nonequilibrium distributions of Figure 6 shows that their shapes compare well up to the maximum but fall off differently at

higher energies. The equilibrium distributions have a smaller high-energy "tail" due to more extensive downscatter from rotational and vibrational excitations. This explains, to some extent, why single-vector projection with "cleanup" performs well on nonequilibrium distributions whose maxima are concentrated at or below about 0.1 eV. The poor similarity observed between equilibrium and nonequilibrium distributions approaching 1 eV at maximum tends to prohibit stationary behavior of projection coefficients at these energies. In fact, collision volume error at these energies is nearly the same for the projection method (with "cleanup") and the conventional method.

The method of selection of a dominant basis vector was the same for an orthogonal basis and for a nonnegative projection basis. The same component is identified in either case. No assumption was made about the form of error induced in the energy distribution function by the erroneous cross-section set used. Several other approaches were tested, including best fit to first and second energy moments (average energy and energy spread), as ways of selecting the dominant basis vector. No significant improvement was found, except that it became clear that knowledge of the type of error could be exploited to produce a superior error reduction. Deliberately using a "hotter" basis vector than indicated caused a better reduction in collision volume error, because of cancellations in error contributed by different parts of the energy distribution. This method was not our objective, yet may be useful in certain circumstances. Thus if models of cross-section error are defined, the method of dominant basis vector selection can be biased to reduce error further than a "blind" method, such as we have used.

Both orthogonal and nonnegative projection methods work about equally well for energy distributions near equilibrium, so that significant error reduction is possible when "cleanup" is added (eq (99)) to the spectral form for ensemble collision volume. Unfortunately both methods serve poorly when the energy distribution is far from equilibrium. For the strong 100-Td electric field, this state is attained within 10 ps, and within 100 ps for a 10-Td electric field. This may be due to the large rotational and vibrational responses above 0.1 eV for air which, in equilibrium, depopulate that portion of the energy spectrum filled by strong electric fields. This hypothesis is strengthened by the fact that ensemble collision volume estimates by the projection method are too low in this regime, presumably because higher energies are underpopulated in equilibrium compared to nonequilibrium. (Higher energies carry a larger collision volume per electron.) Gases that lack such a strong depopulating process may yield better projection method results, although such a case lacks interest. Likewise, distributions substantially above 2 eV in air might avoid this underpopulation effect and yield better nonequilibrium results for the projection method.

The single-vector projection with "cleanup" could have been derived independently of the projection-related theory of this effort, as it is conceptually very simple. It simply trades most of the collision volume calculation using equation (5) for an experimentally measured collision volume represented by equation (9). In the context of its derivation here, the variational properties of the single-vector projection with "cleanup" become apparent. If the error associated with the measurement is as great or greater than the error associated with the energy distribution function, then nothing is gained in accuracy. Generally we expect more accuracy from an equilibrium measurement than from a nonequilibrium calculation.

Although this effort is directed at estimates of ensemble collision volume, the same computational machinery can be applied to other electron swarm properties as well, such as the coefficient of attachment or avalanching. In such a case a weight function equal to that energy-dependent coefficient would be substituted for $K(E)$. The previous conjecture regarding underpopulation at several electron volts applies as well in this case, where poor projection method results would be expected until large spectrum content develops at higher energies. Avalanching, however, does not become important until the spectrum content develops at higher energies.

Nothing has been specified about the source of electrons described by the energy distribution function, up to this point. In nonattaching gas, electrons will linger until absorbed by walls, for example. For attaching gases such as air, a continual source of electrons is required to sustain a significant electron density for times much longer than the attachment time. While an experimental apparatus might generate clouds of near-thermal electrons, there is also the case of electrons produced by ionizing radiation. Such electrons are produced throughout an exposed volume at relatively high energies from 10 to 100 eV. The projection method highlights the possible value of equilibrium measurements of swarm parameters in a volume exposed to constant ionizing radiation. In such a measurement the electric field would be imposed on an ensemble of electrons whose energy distribution incorporates the peculiar spread of electrons throughout higher energies derived from their birth through ionizing radiation. Such equilibrium measurements could shed considerable light on swarm properties of near-equilibrium and nonequilibrium distributions in ionizing radiation.

5 Conclusions

A differential equation has been derived describing the time evolution of the energy distribution function for free electrons in a gas in a transient electric field. A finite-difference approximation and a time-stepping algorithm using matrix-vector techniques were devised to solve the differential equation. An extensive published cross-section set was added to the time-stepping algorithm to enable calculation of realistic energy distribution functions in air. A projection method was described which allows computation of electron swarm properties such as collision volume (related to mobility) using measured data for equilibrium distributions, and the projection method was shown to have desirable variational properties in calculating the swarm properties.

Several projective methods were compared with conventional techniques for their ability to reduce error in estimates of collision volume arising from cross-section-induced error in the energy distribution function, including orthogonal and nonnegative projections. A single-vector projection with "cleanup" of approximation error was found to perform best, leading to a significant reduction of collision volume error when the distribution function maximum was not greater than about 0.1 eV. Other projections performed poorly compared to conventional methods of calculating swarm collision volume, because of the inherent linear dependence of the projection basis of equilibrium distributions and the resulting ill-conditioning of the projection matrix. If a model of the energy dependence of the cross-section error is known, it may be possible to exploit that knowledge to bias the single-vector projection to give better results.

6 Recommendations

Electron mobility estimates for near-thermal (with a peak not greater than 0.1 eV) nonequilibrium energy distributions can be made with greater accuracy using a single-vector projection (onto an equilibrium basis) with "cleanup." Estimates based on the mobility of an equilibrium distribution having the same average energy as the nonequilibrium distribution are a special case of the above without "cleanup."

For electron swarms populated by ionizing radiation, measurements of equilibrium swarm properties in a time-constant electric field and radiation source would likely be very useful and shed new light on swarm properties of nonequilibrium electron distributions arising in this way.

References

[1] Huxley, L. G. H., and R. W. Crompton, *The Diffusion and Drift of Electrons in Gases*, John Wiley and Sons, New York (1974).

[2] Morse, P. M., and H. Feshbach, *Methods of Theoretical Physics*, McGraw-Hill Book Company, Inc., New York (1953), Volume 2, pp 1108f.

[3] Frost, L. S., and A. V. Phelps, Rotational excitation and momentum transfer cross-sections for electrons in H_2 and N_2 from transport coefficients, Phys. Rev. **127** (1962), 1621.

[4] Phelps, L. V., and L. C. Pitchford, Anisotropic scattering of electrons by N_2 and its effect on electron transport, Phys. Rev. **A 31** (1985), 2932.

[5] Carron, N. J., On the Calculation of th Electron Energy Spectrum in a Weakly Ionized Gas, Mission Research Corporation Report MRC-R-1055 (30 January 1987).

[6] Carnahan, B., H. A. Luther, and J. O. Wilkes, *Applied Numerical Methods*, John Wiley and Sons, New York (1969), p 451.

[7] Carter, L. L., and E. D. Cashwell, *Particle-Transport Simulation with the Monte Carlo Method*, USAERDA Publication TID-26607, USAERDA Technical Information Center, Oak Ridge, TN (1975), p 73.

[8] Phelps, A. V., and L. C. Pitchford, Anisotropic Scattering of Electrons by N_2 and its Effects on Electron Transport: Tabulations of Cross Section and Results, JILA Information Center Report No. 26, University of Colorado, Boulder, CO (1 May 1985), p 14.

[9] Phelps, A. V., Tabulations of Collision Cross Sections and Calculated Transport and Reaction Coefficients for Electron Collisions with O_2, JILA Information Center Report No. 28, University of Colorado, Boulder, CO (1 September 1985), p 10.

[10] Goldstein, B., A Summary of Rotational and Vibrational Cross Sections in N_2, Mission Research Corporation Report MRC-R-1057 (26 January 1987).

[11] Wadzinski, H. T., and J. R. Jasperse, Low Energy Electron and Photon Cross Sections for O, N_2, and O_2, and Related Data, Air Force Geophysics Laboratory (PHY), Report AFGL-TR-82-0008 (4 January 1982).

[12] Pitchford, L. C., and A. V. Phelps, Comparative calculations of electron-swarm properties in N_2 at moderate E/N values, Phys. Rev. **A 25** (1982), 540-554.

[13] Dutton, J., A survey of electron swarm data, J. Phys. Chem. Ref. Data, **4** (1975), 577-856.

DISTRIBUTION

ADMINISTRATOR
DEFENSE TECHNICAL INFORMATION
   CENTER
ATTN DTIC-DDA (2 COPIES)
CAMERON STATION BUILDING 5
ALEXANDRIA, VA 22304-6145

UNDER SECRETARY OF DEFENSE
   RESEARCH & ENGINEERING
ATTN TECHNICAL LIBRARY, 3C128
WASHINGTON, DC 20301

COMMANDER
ATMOSPHERIC SCIENCES LABORATORY
ATTN TECHNICAL LIBRARY
WHITE SANDS MISSILE RANGE, NM 88002

DIRECTOR
US ARMY BALLISTIC RESEARCH
   LABORATORY
ATTN SLCBR-DD-T (STINFO)
ABERDEEN PROVING GROUND, MD 21005

US ARMY ELECTRONICS TECHNOLOGY &
   DEVICES LABORATORY
ATTN SLCET-DD
FT MONMOUTH, NJ 07703

DIRECTOR
US ARMY MATERIEL SYSTEMS ANALYSIS
   ACTIVITY
ATTN AMSY-MP
ABERDEEN PROVING GROUND, MD 21005

DIRECTOR
NATIONAL INSTITUTE OF STANDARDS
   & TECHNOLOGY
ATTN LIBRARY
WASHINGTON, DC 20234

DIRECTOR
DEFENSE NUCLEAR AGENCY
ATTN TISI-SCIENTIFIC INFORMATION
      DIV
ATTN RAAE, ATMOSPHERIC EFFECTS
      DIV
ATTN RAEV, ELECTRONICS VULNERABILITY
      DIV
WASHINGTON, DC 20305

COMMANDER OFFICER
US ARMY FOREIGN SCIENCE &
   TECHNOLOGY CENTER
FEDERAL OFFICE BLDG
ATTN AMXST-SC, SCIENCES DIV
220 7TH STREET, NE
CHARLOTTESVILLE, VA 22901

DIRECTOR
US ARMY MISSILE LABORATORY
USAMICOM
ATTN DRSMI-RPT, TECHNICAL
      INFORMATION DIV
REDSTONE ARSENAL, AL 35809

COMMANDER
US ARMY NUCLEAR & CHEMICAL AGENCY
ATTN ATCN-W, WEAPONS EFFECTS DIV
BACKLICK ROAD, BUILDING 2073
SPRINGFIELD, VA 22150

US CHIEF OF ARMY RESEARCH OFFICE
ATTN DRXRO-MA, DIR MATHEMATICS DIV
ATTN DRXRO-PH, DIR PHYSICS DIV
ATTN M. CIFTAN
RESEARCH TRIANGLE PARK, NC 27709

CHIEF OF NAVAL RESEARCH
DEPT OF THE NAVY
ATTN ONR-400, ASST CHIEF FOR RESEARCH
ATTN ONR-420, PHYSICAL SCI DIV
ARLINGTON, VA 22217

DIRECTOR
NAVAL RESEARCH LABORATORY
ATTN 2600, TECHNICAL INFO DIV
ATTN 6000, MATL & RAD SCI & TE
WASHINGTON, DC 20375

COMMANDER
NAVAL SURFACE WEAPONS CENTER
ATTN F-30, NUCLEAR EFFECTS DIV
ATTN R-40, RADIATION DIV
ATTN E-43, TECHNICAL LIB
WHITE OAK, MD 20910

AIR FORCE OFFICE OF SCIENTIFIC
      RESEARCH
ATTN DR. R. BARKER
BOLLING AIR FORCE BASE
WASHINGTON, DC 20332-6448

UNIVERSITY OF COLORADO
NIST & DEPT OF PHYSICS, QUANTUM
   PHYSICS DIV
ATTN DR. A. V. PHELPS
BOULDER, CO 80309

SANDIA NATIONAL LABORATORIES
ATTN DIVISION 4211, DR. L. C. PITCHFORD
ALBUQUERQUE, NM 87185

SUPERINTENDENT
HQ, US AIR FORCE ACADEMY
ATTN TECH LIB
USAF ACADEMY, CO 80840

LIVERMORE LABORATORY
PO BOX 969
LIVERMORE, CA 94550

SANDIA NATIONAL LABORATORIES
PO BOX 5800
ALBUQUERQUE, NM 87185

GEORGIA STATE UNIVERSITY
ATTN PHYSICS & ASTRONOMY DEPT,
    DR. S. MANSON
UNIVERSITY PLAZA
ATLANTA, GA 30303-3083

PACIFIC NORTHWEST LABORATORY
ATTN RADIOLOGICAL SCIENCES DEPT,
    DR. J. MILLER
RICHLAND, WA 99352

METATECH CORPORATION
ATTN DR. C. JONES
2309 RENARD PLACE, SE, SUITE 401
ALBUQUERQUE, NM 87106

MISSION RESEARCH CORPORATION
ATTN DR. N. CARRON
735 STATE STREET, PO DRAWER 719
SANTA BARBARA, CA 93102

US ARMY LABORATORY COMMAND
ATTN TECHNICAL DIRECTOR, AMSLC-TD

INSTALLATION SUPPORT ACTIVITY
ATTN LEGAL OFFICE, SLCIS-CC

USAISC
ATTN RECORD COPY, AMSLC-IM-TS
ATTN TECHNICAL REPORTS BRANCH
    AMSLC-IM-VP (2 COPIES)

HARRY DIAMOND LABORATORIES
ATTN D/DIVISION DIRECTORS
ATTN CHIEF SCIENTIST, SLCHD-CS
ATTN LIBRARY, SLCHD-TL (3 COPIES)
ATTN LIBRARY, SLCHD-TL (WOODBRIDGE)
ATTN CHIEF, SLCHD-NW-CS
ATTN CHIEF, SLCHD-NW-E
ATTN CHIEF, SLCHD-NW-EH
ATTN CHIEF, SLCHD-NW-EP
ATTN CHIEF, SLCHD-NW-ES
ATTN CHIEF, SLCHD-NW-P
ATTN CHIEF, SLCHD-NW-R
ATTN CHIEF, SLCHD-NW-RP
ATTN CHIEF, SLCHD-NW-RS
ATTN CHIEF, SLCHD-NW-TN
ATTN CHIEF, SLCHD-NW-TS
ATTN CHIEF, SLCHD-HPM (2 COPIES)
ATTN KENYON, C. S., SLCHD-NW-EP
ATTN MERKEL, G., SLCHD-NW-TN
ATTN WYATT, W. T., SLCHD-NW-EP (30 COPIES)